AN ALL-OPTICAL PULSE REGENERATOR

By

Najeeb Haddad

Bachelor of Science

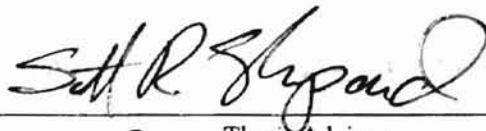**Mu'tah University**

Mu'tah, Jordan

1991

Submitted to the Faculty of the
Graduate College of the
Oklahoma State University
in partial fulfillment of
the requirements for
the Degree of
MASTER OF SCIENCE
May, 1999
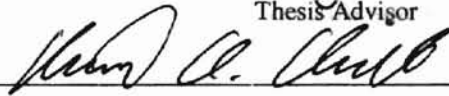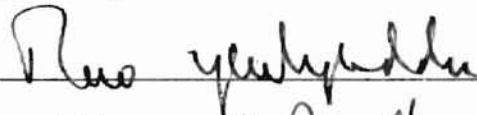
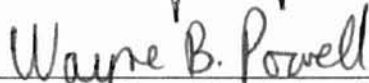# AN ALL-OPTICAL PULSE REGENERATOR

Thesis Approved:

_____
Thesis Advisor

_____

_____

_____
Dean of the Graduate College

ACKNOWLEDGMENTS

I wish to express my sincere appreciation to my advisor, Dr. Scott Shepard, for the original conception, continuous guidance, and tremendous supervision of this study. I would like to thank my other committee members, Dr. R. K. Yarlagadda and Dr. Allen Cheville for their assistance and guidance. I wish also to express my gratitude for Dr. Daniel Grischkowsky, Dr. George Scheets, Dr. Gary Yen, Dr. Kenneth Church, and Dr. Albert Rosenbrger for their teaching me the concepts of telecommunications and optics.

I would like to give my special and lasting appreciation to my father, my mother, my sisters and my brothers for their magnificent love and support. I would like to express my sincere gratitude to my sister, Manal, and her husband, Jawdat Zeidan, for their constant care and enormous support. Thanks also go to my uncle, Noor Haddad, for his encouragement and enduring support. My thanks extend to my sister, Neli, for her taking care of me in the last four months of writing this thesis.

Finally, I would like to thank the department of Electrical and Computer Engineering for their supporting during these two years of study.

TABLE OF CONTENTS

LIST OF FIGURE

NOMENCLATURE

EDFAs	Erbium Doped Fiber Amplifiers
$w(t)$	pulse energy per unit area
I	light intesity
w_s	saturation energy
N_1	population intensity in the energy state 1
N_2	population intensity in the energy state 2
υ_g	group velocity
α_0	unsaturable constant loss through the amplifier
σ	emission (absorption) cross section
l_g	the saturable absorber/amplifier length
γ_0	the small signal gain
G_0	the small signal gain $\exp[-\gamma_0 l_g]$
κ	the coupling constant
$\bar{P}(\bar{r},t)$	the total medium polarization
$\bar{E}_y(\bar{r},t)$	the electric field in the perturbed waveguide
A_m	the mth mode amplitude
$G\ (>0)$	the amplitude gain (of the mth mode) per unit length

$L \ (>0)$	the amplitude loss (of the mth mode) per unit length
β	propagation constant
$\bar{P}$	polarization.
Ω	the transition frequency.
T_2	the transverse, dipole-dipole, or spin-spin relaxation time.
T_1	the longitudinal, spin-lattice, or dipole-lattice relaxation time
$N_1 - N_2 \equiv N$	population inversion (difference between state 1 and state 2 in a two-level a atomic system)
μ_{12}	total dipole moment
$(N_1 - N_2)^\epsilon$	the equilibrium population inversion.
η	damping coefficient so that in the absence of polarization the energy of the plane wave, which proportional to $\left| \vec{E} \right|^2$, decays as $\exp[-\eta z]$ for propagation in the z direction
I_{sat}	saturation intensity
$I_{sat(G)}$	saturation intensity of the amplifying waveguide
$I_{sat(L)}$	saturation intensity of the lossy waveguide
$g_L(\omega, \Omega)$	the Lorentzian line-shape factor
$\Delta \omega_L$	the characteristic linewidth for the Lorentzian line
k	the propagation constant
G^ϵ	equilibrium value of the gain (the perturbing electric field is absent)
L^ϵ	equilibrium value of the loss (the perturbing electric field is absent)
G	gain per unit length

L	loss per unit length
a_1, a_2	normalized mode amplitudes
l	normalized loss per unit length
g	normalized gain per unit length
l_0	normalized equilibrium value of the loss
g_0	normalized equilibrium value of the gain
K	normalized coupling coefficient
y	normalized time parameter
x	normalized space parameter
r	real part of the mode amplitude a_1
s	imaginary part of the mode amplitude a_1
t	real part of the mode amplitude a_2
u	imaginary part of the mode amplitude a_2
f	a parameter to indicate how small or big is the gain saturation compared to the loss saturation (i.e., $I_{sat(G)} / I_{sat(L)}$)
$s(x, y)$	the characteristic direction along which the mode amplitudes propagate
δs	the step length along the s direction
δy	the step length along the y direction (δy on the plots is dy)
A	the input pulse amplitude
τ	a normalized time constant that determines the rising/dropping time of the leading/trailing edge of the input pulse and it also determines the pulse width

INTRODUCTION

Recent developments and research in the field of integrated optics has expanded because of the need of such devices in the vast and rapidly growing use of optical fiber in telecommunications systems. High data rates (>1 Gb/s) and the expenses of electronic processing at these speeds are motivating the development of all-optical components (such as switches, modulators, demodulators, amplifiers, and regenerators). Consider for example the use of Erbium Doped Fiber Amplifiers (EDFAs) in long distance transmission systems.

1.1 Erbium Doped Fiber Amplifiers (EDFAs)

These all-optical amplifiers eliminate the cost of performing optical to electronic to optical conversions and the cost and reliability drawbacks of electronic amplifiers. Since an EDFA provides gain at 1.55 μm by creating a population inversion via an optical pump at 980 nm, the supply of power to these amplifiers has advantages over their electronic counter parts. This feature makes EDFAs indispensable for transoceanic fiber links as well as cost effective for land based systems [1].

The noise performance is found to be virtually quantum-limited and this permits hundreds of amplifiers to be cascaded without significant degradation. The interactions of fiber nonlinear effects of Self-Phase Modulation (SPM) and Four-Wave Mixing (FWM) with signal and Amplified Spontaneous Emission (ASE) noise will render ultra-long-distance transmission (>100 Km) of non-return to zero (NRZ) signals very difficult at data rates

higher than 10 Gb/s. An EDFA can support many wave division multiplexing (WDM) channels and the total capacity is limited by the nonlinear effects in the transmission fiber [1].

Currently deployed systems utilize up to 40 different wavelengths, and 100 wavelength systems are being planned [2]. Capacities of systems utilizing EDFAs vary but it is not uncommon for these to carry 24 OC-48 signals (yielding a total capacity of 59.7 Gb/s).

1.2   Regenerators

A significant advantage for using all-optical transmission is that digital signals lend themselves to periodic conditioning and reshaping. Thus each repeater can be used to regenerate the pulse waveforms at each sample time. This type of repeater is called a regenerative repeater.

A regenerator is different than an amplifier since it can actually remove noise and/or distortion from a signal by using a nonlinear decision element or "slicer". The signal is "sliced" by setting a threshold: anything above this threshold is decided to be a one; anything below it is decided to be a zero. The regenerated signal that is output is then clamped to be exactly the amplitude chosen for a one (or zero) for regions where the input signal was decided to be a one (or zero). Thus regenerators can remove the effects of dispersion in fiber systems (if spaced closely enough) whereas EDFAs, being merely amplifiers, can not. Removing dispersion can either increase capacity at fixed length or increase lengths at fixed capacity.

The choice between regenerators or amplifiers is a key technological issue that motivates network architectures and possible services [3]. Presently, to regenerate an optical signal one

2

must go through the very expensive process of: optical to electronic conversion; fanning out

the high capacity signal to many lower data rate electronic signal; then recombining these

regenerated signals into the high capacity optical signal. To produce an all-optical regenerator

is recognized as a key step towards all-optical networking [4].

Chapter 2

SATURABLE AMPLIFIERS/ABSORBERS

The saturable amplifier/absorber is a non-linear material that is amplifying/attenuating when the light propagating through it has a low intensity, and highly transparent when the light has a high intensity.

Verdeyen [5] has discussed the pulse propagation in saturable amplifiers and absorbers. This discussion is important here since our device couples a gain medium to an attenuating one and both media may exhibit saturation. This coupling is performed to help us balance the gain and loss at some value. Verdeyen's discussion is presented in this chapter to give us an idea how these saturable amplifiers/absorbers affect the pulses propagating through them.

Verdeyen has discussed short duration pulses (its time duration is much less than any characteristic time scales in the atomic system interacting with the pulse). These pulses carry energy per unit area of w(t) (joules/area).

The intensity will change because of variations in time, space, and the inversion, which is also a function of (z', t')

$$\frac{\partial I}{\partial z'} + \frac{1}{v_g} \frac{\partial I}{\partial t'} = \Delta N(z', t') \sigma I(z', t') - \alpha_0 I(z', t'), \tag{2.1}$$

$t' \equiv$ time kept by a universal clock,

$\Delta N(t') = N_2(t') - N_1(t')$,

$N_2 \equiv$ population intensity in the energy state 2,

$N_1 \equiv$ population intensity in the energy state 1,

$\upsilon_g \equiv$ group velocity,

$\alpha_0 \equiv$ unsaturable constant loss through the amplifier,

$\sigma \equiv$ emission (absorption) cross section.

Using the transformation $z = z', t = t' - z/\upsilon_g$ to measure time after the arrival of the leading edge of the pulse, equation (2.1) becomes

$$\frac{\partial I}{\partial z} = [N_2(z,t) - N_1(z,t)]\sigma I(z,t) - \alpha_0 I(z,t). \tag{2.2}$$

$N = N_2 + N_1$ does not change with time and assumed to be independent of z.

$$\frac{\partial N_2}{\partial t} = \frac{(N_2 - N_1)\sigma I}{h\nu} = \frac{-2\sigma I}{h\nu}N_2 + \frac{\sigma I}{h\nu}N, \tag{2.3a}$$

or

$$\frac{\partial N_2}{\partial t} + \frac{\sigma I}{h\nu}N_2 = \frac{\sigma I}{h\nu} = \frac{N}{2}\frac{\sigma I}{h\nu}, \tag{2.3b}$$

$$w(t) = \int_{-\infty}^{t} I(z,t')dt'. \tag{2.4}$$

From Eq(2.4) we get

$$I(z,t) = \dot{w}(z,t). \tag{2.5}$$

Normalizing $w(z,t)$ to the saturation energy $w_s = \dfrac{h\nu}{2\sigma}$, we get

$$u(z,t) = \frac{w(z,t)}{w_s}. \tag{2.6}$$

Substituting equations (2.5) and (2.6) in equation (2.3) we get

$$\frac{\partial N_2}{\partial t} + \dot{u}N_2 = \frac{N}{2}\dot{u}. \tag{2.7}$$

The solution for equation (2.7) is

$$N_2(z,t) = \frac{N}{2} + K \exp[-u(z,t)],$$ (2.8)

where K is the constant of integration evaluated by the initial conditions (before the arrival of the pulse) the energy and the population inversion. At $t = -\infty$ the energy is zero, $N_2 = N_2^0$, and $N_1 = N_1^0$, where $N_2^0 + N_1^0 = N$ is a constant. Using these initial conditions, the integration constant $K = \frac{\Delta N^0}{2}$, equation (2.8) can be written as

$$N_2(t) - N_1(t) = \Delta N(t) = \Delta N^0 \exp[-u(t)].$$ (2.9)

Multiplying (2.9) by the gain cross section, substituting it into (2.2), and dividing by the saturation energy, we get

$$\frac{\partial}{\partial t}\dot{u}(z,t) = \gamma_0 \dot{u}(z,t)\exp[-u(z,t)] - \alpha_0 \dot{u}(z,t),$$ (2.10)

where $\gamma_0 = \Delta N^0 \sigma$ is the small signal gain coefficient (at $t = -\infty$). Integrating equation (2.10) with respect to time we get

$$\frac{\partial}{\partial t}u(z,t) = \gamma_0[1 - \exp[-u(z,t)]],$$ (2.11)

where we assumed that the unsaturable loss α_0 is zero for simplicity.

Figure (2.1) shows a saturable amplifier/absorber with length l_g. Integrating equation (2.11) with respect to the distance z between the input plane (1) and the output plane (2), as shown in figure (2.1), we get

$$\int_{u_1}^{u_2} \frac{du}{1 - e^{-u}} = \gamma_0 \int_0^{l_g} dz = \gamma_0 l_g = \ln G_0,$$

6

where $G_0 \equiv$ the small signal gain $\exp[-\gamma_0 l_g]$. The solution of the above integral, after some rearrangements, is

$$\exp[u_2(t)] = 1 + G_0(\exp[u_1(t)] - 1).$$ (2.12)

Differentiating (2.12) with respect to the local time, multiplying both sides by w_s and then using (2.12) for $\exp[u_2(t)]$ gives

$$w_s \dot{u}_2 = \frac{w_s G_0 \dot{u}_1 \exp[u_1(t)]}{1 + G_0(\exp[u_1(t)] - 1)},$$

which gives the output intensity in terms of the input intensity as follows

$$I_2(t) = I_1(t) \frac{G_0 \exp[u_1(t)]}{1 + G_0[\exp[u_1(t)] - 1]}.$$ (2.13)

In case of saturable amplifier $G_0 > 1$ and in case of saturable absorber $G_0 < 1$.

Let the input intensity at plane 1 in Figure (2.1) be given by

$$I_1(t) = \frac{w_0}{T} \sin^2(\frac{\pi t}{2T}) \qquad\qquad 0 < t < 2T$$

where w_0 is the total energy in the pulse. Figure (2.2) shows the output $I_2(t)$ divided by the peak input intensity (w_0 / T) for various values of w_0 / w_s for $G_0 = 4$ (i.e., 6dB) and for a 6dB attenuater. As seen from Figure (2.2) in the case of small values of w_0 / w_s, the output is amplified/attenuated by a factor of 4. For w_0 / w_s equals to ~ 1 to 2, the pulse shape is quite distorted. In the case of saturable amplifier the leading edge is affect completely by the gain but the output will saturate the amplifier and the trailing edge will face less amplification and thus the "risetime" of the pulse is shortened. Decreasing amplification/absorption with increasing intensity is called bleaching. For the case of saturable absorber the output bleaches the absorption and the trailing edge of the pulse is sharpened since it is less affected

7

by the attenuation than the leading edge. These differences between an amplifier and absorber play the basic role in our device.
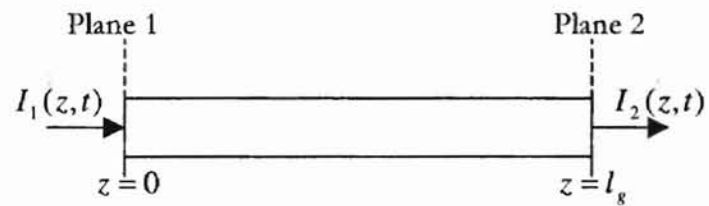

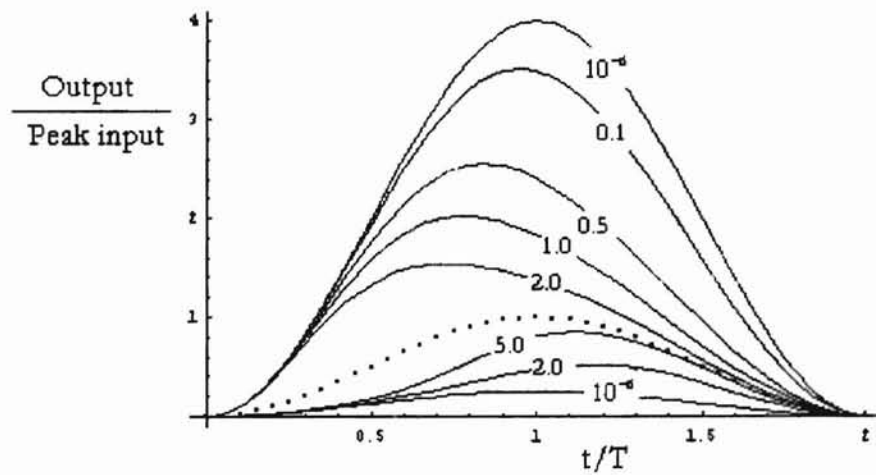**FIGURE 2.1:** Saturable absorber/amplifier medium.

FIGURE 2.2: The relative transmission through a saturable amplifier/absorber.

THE FORMULATION

OF THE MATHEMATICAL MODEL

Our device consists of two evanescently coupled optical waveguides. One of these waveguides is lossy and the other is amplifying. In this section the equations that govern the behavior of light signals traveling through this device are derived. These equations are derived in the semiclassical manner. This semiclassical treatment does not use quantum theory to describe the radiation field but instead treats the electromagnetic field as classical force acting on the atomic system providing the gain (attenuation) mechanism. This approximation yields highly accurate results when applied to standard (coherent state) laser light fields at frequencies within the visible light spectrum and is valid for actual devices at intensities capable of saturating a nonlinear medium [6].

In section 3.1 a time dependent coupled mode theory is developed. Two equations that describe the transient behavior of the mode amplitudes of waves traveling through a two-coupled single-mode slab dielectric waveguides are derived. In section 3.2 the interaction of electromagnetic energy with atoms is described and two rate equations for both waveguides are derived. Then a dimensionless form of the four dynamic equations is defined.

3.1 Coupled Mode Theory in Space and Time

Pierce *et al.* [7] introduced the original work of coupling of modes. Energy coupling between parallel channels has been discussed extensively in the past [8] and reformulated lately by several groups under the title of "improved coupling mode theory" [9]-[12]. The coupled mode theory for optical waveguides was developed by Marcuse [13], Synder [14][15], Yariv and Taylor [16]. Many other papers have also been published: discussing different applications to the coupled mode theory in all optical and in optoelectronic devices such as optical directional couplers; TE/TM polarization converters; optical filters; modulators; multiplexers; demultiplexers; etc. Many of these applications are well documented and summarized in [17].

Coupled mode theory is approximate, with approximations that are not always self-evident [18]. In 1958, H. A. Haus showed that the coupled mode theory is derivable from a variational expression for the propagation constant [19].

Here Yariv's formalism [20] that describes exchange of power between modes is used. In his development, Yariv assumed that the mode amplitudes are time invariant. Since we study the transient behavior of coupled waveguides, Yariv's formulation needs to be extended to consider time and space variant mode amplitudes.

Starting with the wave equation

$$\nabla^2 \vec{E}(\vec{r},t) = \mu \varepsilon_0 \frac{\partial^2 \vec{E}(\vec{r},t)}{\partial t^2} + \mu \frac{\partial^2 \vec{P}(\vec{r},t)}{\partial t^2},$$

(3.1)

where $\vec{P}(\vec{r},t)$ is the total medium polarization and can be taken as the sum

$$\vec{P}(\vec{r},t) = \vec{P}_0(\vec{r},t) + \vec{P}_{Pert}(\vec{r},t)$$

(3.2)

and

$$\bar{P}_0(\bar{r},t) = [\varepsilon(\bar{r}) - \varepsilon_0]\bar{E}(\bar{r},t) \tag{3.3}$$

is the polarization induced by $\bar{E}(\bar{r},t)$ in the *unperturbed* waveguide whose dielectric constant

is $\varepsilon(\bar{r})$. $\bar{P}_{Pert}(\bar{r},t)$ is then defined by (3.2) and represents any deviation of the polarization

from that of the unperturbed waveguide due to the external force, the bianisotropy of the

medium, corrugations in the waveguide surface, or whatever else might be causing the

deviation between $\bar{P}$ and $\bar{P}_0$. Systems in which polarization of this more general form

occurs may be analyzed in terms of coupled modes.

Using (3.2) and (3.3) in (3.1) gives

$$\nabla^2 \bar{E}_y - \mu\varepsilon(\bar{r})\frac{\partial^2 \bar{E}_y}{\partial t^2} = \mu\frac{\partial^2 [\bar{P}_{Pert}(\bar{r},t)]_y}{\partial t^2} \tag{3.4}$$

and similar expressions for $\bar{E}_x$ and $\bar{E}_z$.

Ignoring the possibility of coupling to the continuum of radiation modes, the electric

field in the "perturbed" waveguide may be expanded as a superposition of confined modes.

For example, considering only plane waves that travel in the $+z$ direction,

$$\bar{E}_y(\bar{r},t) = \frac{1}{2}\mathrm{Re}\{\sum_m A_m(z)E_y^{(m)}(x)\exp[i(\omega t - \beta_m z)]\}, \tag{3.5}$$

where the mode amplitudes A_m are allowed to vary with z. To determine the transient

behavior of the mode amplitudes due to the turning on or off, or temporal variation of the

perturbation, one must allow for the time dependence of the mode amplitudes, thus

$$\bar{E}_y(\bar{r},t) = \frac{1}{2}\mathrm{Re}\left\{\sum_m A_m(z,t)E_y^{(m)}(x)\exp[i(\omega t - \beta_m z)]\right\}. \tag{3.6}$$

Assuming "slowly" varying envelope (the mode amplitudes vary only slightly over a distance

of an optical wavelength and within a time interval of an optical period) so that

$$\left| \frac{\partial^2 A_m(z,t)}{\partial z^2} \right| << \left| \beta_m \frac{\partial A_m(z,t)}{\partial z} \right|$$

and

$$\left| \frac{\partial^2 A_m(z,t)}{\partial t^2} \right| << \left| \omega \frac{\partial A_m(z,t)}{\partial t} \right|$$

equation (3.6) can be written as

$$\text{Re}\left\{ \sum_m [-i\beta_m \frac{\partial A_m}{\partial z} E_y^{(m)}(x)\exp[i(\omega t - \beta_m z)] - i\omega\mu\varepsilon \frac{\partial A_m}{\partial t} E_y^{(m)}(x)\exp[i(\omega t - \beta_m z)]] \right\} =$$

$$\mu \frac{\partial^2 [\vec{P}_{Pert}(\vec{r},t)]_y}{\partial t^2}. \tag{3.7}$$

Since the modes $E_y^{(m)}$ are orthogonal, we have

$$\int_{-\infty}^{\infty} E_y^{(l)}(x) E_y^{(m)}(x) dx = \frac{2\omega\mu}{\beta_m} \delta_{l,m}. \tag{3.8}$$

Multiplying (3.7) by $E_y^{(l)}$ and integrating from $-\infty$ to ∞. The result, using (3.8), is

$$\frac{\partial A_m}{\partial z} + \frac{\omega\mu\varepsilon}{\beta_m} \frac{\partial A_m}{\partial t} = \frac{i}{2\omega} \frac{\partial^2}{\partial t^2} \left\{ \int_{-\infty}^{\infty} [\vec{P}_{Pert}(\vec{r},t)]_y E_y^{(m)}(x) dx \right\}. \tag{3.9}$$

The term on the right hand side of the above equation is a source term, i.e., it represents energy that is either imparted to or taken from the energy of the mth mode due to the presence of the perturbation.

Two cases important to our proposed device are discussed here to analyze the source term. First, consider the case of a single isotropic waveguide. Suppose a perturbation is induced in the form of an external pump to achieve a population inversion that causes light wave amplification. In the steady state the mode amplitudes are assumed not to vary in time and (3.9) can be written as:

$$\frac{\partial A_m}{\partial z} = \frac{i}{2\omega} \frac{\partial^2}{\partial t^2} \left\{ \int_{-\infty}^{\infty} [\bar{P}_{Pert}(\bar{r},t)]_y E_y^{(m)}(x)dx \right\}. \tag{3.10}$$

Neglecting gain saturation, equation (3.10) can be written as $\frac{dA_m}{dz} = GA_m$, where the source term takes the form GA_m, and G (>0) is the amplitude gain (of the mth mode) per unit length. Similarly if the medium had nonsaturating losses, then the following equation would hold $\frac{dA_m}{dz} = LA_m$, where L (>0) is the loss per unit length.

In case of saturable amplifier/absorber medium the above equations would still hold except that G and L would become functions of z. To solve for the mode amplitude we need to combine the above mode equations with the steady state rate equations that describe the medium saturation effects.

The second case is the uniform structure that consists of two adjacent waveguides. We will consider the case where the waveguides are adjacent to each other closely enough that the evanescent fields from each waveguide extend slightly into the other waveguide. The energy of this evanescent field can be considered as an external source term that perturbs or couples energy to the propagating modes of the waveguide that it has penetrated into. The energy that is added or subtracted is proportional to the perturbing evanescent field that is proportional to the mode amplitude of the other waveguide.

Consider two waves (each travels in one of the waveguide), with the implicit time dependence $\exp[-j\beta_1 t]$ that, uncoupled, have the spatial dependences $\exp[-j\beta_1 z]$ and $\exp[-j\beta_2 z]$, respectively. Considering a uniform structure, the propagation constants of the waves, β_1 and β_2, must be of same sign and approximately equal, if the waves are to affect each other [18].

We will consider the case when the two modes are phase matched. For the uniform structures, the phase matching requires that $\beta_1 = \beta_2$. Under phase matching, the coupled mode equations assume the simpler form:

$$\frac{dA_1}{dz} = \kappa A_2, \tag{3.11a}$$

$$\frac{dA_2}{dz} = -\kappa A_1, \tag{3.11b}$$

where A_1 and A_2 are the amplitudes of the single modes of propagation (one for each of the two waveguides) and κ is the coupling constant. The selection of the sign of the source terms in (3.11) is arbitrary as long as one is positive and the other is negative, as may be proved by power conservation arguments for modes traveling in the same direction, or from evaluating the time derivatives of the polarization integral [6].

For two closely adjacent single mode waveguides, one of which is amplifying and the other is lossy (not described by ε) the dynamic behavior is governed by

$$\frac{\partial A_1}{\partial z} + \frac{1}{v_g}\frac{\partial A_1}{\partial t} = GA_1 + \kappa A_2, \tag{3.12}$$

$$\frac{\partial A_2}{\partial z} + \frac{1}{v_g}\frac{\partial A_2}{\partial t} = -LA_2 - \kappa A_1, \tag{3.13}$$

where the unperturbed speed of propagation $v_g = \dfrac{\beta}{\omega\mu\varepsilon}$ is assumed the same for the two waveguides. The time dependence of the mode amplitudes allows the source terms be time dependent also which makes $L = L(z,t)$ and $G = G(z,t)$.

3.2   Gain and Loss Saturation Rate Equations

To analyze saturation of both the loss and the gain media the semicalssical approach is used. In this approach, the field remains classical, but atom is quantized. The interconnection between media and fields is provided by the electric dipole interaction.

The interaction that takes place between a classical electromagnetic field and a quantized medium by means of the electric dipole transition can be described by a set of coupled nonlinear differential equations which as derived in [21] are:

$$\ddot{\bar{P}} + \frac{2}{T_2}\dot{\bar{P}} + \Omega^2 \bar{P} = \frac{-2\Omega}{\hbar} M \frac{|\mu_{12}|^2}{3}(N_1 - N_2)\bar{E}, \tag{3.14}$$

$$\frac{\partial}{\partial t}(N_1 - N_2) + \frac{(N_1 - N_2) - (N_1 - N_2)^e}{T_1} = -\frac{2}{\hbar\Omega}\dot{\bar{P}}\cdot\bar{E}, \tag{3.15}$$

and

$$\bar{\nabla}\times(\bar{\nabla}\times\bar{E}) + \frac{n\eta}{c}\frac{\partial\bar{E}}{\partial t} + \frac{n^2}{c^2}\frac{\partial^2\bar{E}}{\partial t^2} = -\mu_0 \frac{\partial^2\bar{P}}{\partial t^2}, \tag{3.16}$$

where

$\bar{P} \equiv$ polarization.

$\Omega \equiv$ the transition frequency.

$T_2 \equiv$ the transverse, dipole-dipole, or spin-spin relaxation time.

$T_1 \equiv$ the longitudinal, spin-lattice, or dipole-lattice relaxation time.

$N_1 - N_2 \equiv N \equiv$ population inversion (difference between state 1 and state 2 in a two-level atomic system).

$\mu_{12} \equiv$ total dipole moment.

$$M = \left[\frac{n+2}{3}\right]^2.$$

15

$(N_1 - N_2)^e \equiv$ the equilibrium population inversion.

$\eta \equiv \dfrac{\mu_0 \sigma c}{n} \equiv$ damping coefficient so that in the absence of polarization the energy of the

plane wave, which proportional to $\left|\vec{E}\right|^2$, decays as $\exp[-\eta z]$ for propagation in the

z direction where σ is the absorption cross section.

To study the saturation we start with

$$\frac{\partial}{\partial t}(N_1 - N_2) + \frac{(N_1 - N_2) - (N_1 - N_2)^e}{T_1} = -\frac{2}{\hbar\Omega}\dot{\vec{P}} \cdot \vec{E}. \tag{3.15}$$

The first term on the left-hand side of (3.15) represents power being delivered to the dipole

system, the second term on the left-hand side represents the net power interchange with the

surrounding medium, and the right-hand side corresponds to the power delivered by the

applied field.

In the absence of an applied field $\vec{E}$, the steady-state solution to the population

difference is:

$$(N_1 - N_2) = (N_1 - N_2)^e.$$

For plane wave propagation in the z direction, we assume a solution to (3.14) of the

form

$$\vec{P} = \frac{1}{2}\tilde{P}\exp[i(\omega t - kz)] + C.C. \tag{3.17a}$$

$$\vec{E} = \frac{1}{2}\tilde{E}\exp[i(\omega t - kz)] + C.C. \tag{3.17b}$$

where $C.C.$ denotes the complex conjugate and the tilde ($\sim$) indicates a complex amplitude.

Assuming traveling waves of the form (3.17) for $\vec{P}$ and $\vec{E}$ and equating the time-

independent components on either side of (3.15), we obtain:

$$\frac{\hbar\Omega}{2}\frac{(N_1-N_2)-(N_1-N_2)^e}{T_1}=\frac{-i\omega}{4}(\tilde{P}\cdot\tilde{A}^*-\tilde{P}^*\cdot\tilde{A}),\tag{3.18}$$

where the asterisk denotes the complex conjugate. Since the polarization can be expressed in terms of the field as:

$$\tilde{P}=\varepsilon_0\chi(\omega)\tilde{A}=\varepsilon_0[\chi'(\omega)+i\chi''(\omega)]\tilde{A},$$

equation (3.18) can be written as;

$$\frac{\hbar\Omega}{2}\frac{(N_1-N_2)-(N_1-N_2)^e}{T_1}=\frac{1}{2}\Omega\chi''(\omega)\left|\tilde{A}\right|^2.\tag{3.19}$$

The susceptibility can be eliminated from (3.19) with the aid of

$$\chi''(\omega)=-\frac{\pi}{\hbar\varepsilon_0}M\frac{\left|\mu_{12}\right|^2}{3}(N_1-N_2)\left[\frac{1}{\pi}\frac{1/T_2}{(\Omega-\omega)^2+(1/T_2)^2}\right],\tag{3.20}$$

yielding, for the homogeneously broadened line,

$$(N_1-N_2)=\frac{(N_1-N_2)^e}{1+\dfrac{I}{I_{sat}}\dfrac{g_L(\omega,\Omega)}{T_2/\pi}},\tag{3.21}$$

where $I=\dfrac{n\varepsilon_0 c}{2}\left|\tilde{A}\right|^2$ is the power per unit area carried by the wave, and

$$I_{sat}\equiv\frac{n\varepsilon_0 c}{(2T_1T_2/\hbar^2)M(\left|\mu_{12}\right|^2/3)}\tag{3.22}$$

is referred to as the saturation intensity which is the power per unit area that a wave on resonance must carry in order to reduce the population difference to one-half its unsaturated value.

$g_L(\omega,\Omega)$ is the Lorentzian line-shape factor and is given by

$$g_L(\omega,\Omega)=\frac{1}{\pi}\frac{1/T_2}{(\Omega-\omega)^2+(1/T_2)^2}.\tag{3.23}$$

17

The characteristic linewidth for the Lorentzian line, $\Delta\omega_L$, is given by

$$\Delta\omega_L = \frac{2}{T_2} \tag{3.24}$$

where $\Delta\omega_L$ is the frequency difference between the points on either side of the central maximum where $g_L(\omega,\Omega)$ drops to one-half its line-center value and is called the full width at half maximum (FWHM).

In our case, we assume a resonant $(\omega = \Omega)$ traveling wave of the form (3.17) incident on a medium (with loss or gain). We are considering propagating wave solutions that are steady-state oscillations in time of frequency Ω but are allowed to vary slowly in space and time through the complex amplitudes $\tilde{P}(z,t), \tilde{A}(z,t)$. The quantity k in (3.17) is the propagation constant, $k \equiv \dfrac{\Omega n}{c} \equiv \dfrac{\omega n}{c}$.

Substituting of (3.17) into (3.14) and (3.15) yields

$$\tilde{P}(z) = \frac{-iT_2}{\hbar} M \frac{|\mu_{12}|^2}{3} N\tilde{A} \tag{3.25}$$

$$\dot{N} + \frac{(N - N^e)}{T_1} = \frac{-i}{2\hbar}(\tilde{P} \cdot \tilde{A}^* - \tilde{P}^* \cdot \tilde{A}), \tag{3.26}$$

where $N \equiv N_1 - N_2$.

In deriving the above equations the slowly varying wave assumption $\left|\dfrac{\partial^2 \tilde{A}}{\partial z^2}\right| << \left|k \dfrac{\partial \tilde{A}}{\partial z}\right|$

and $\left|\dfrac{\partial^2 \tilde{A}}{\partial t^2}\right| << \left|\omega \dfrac{\partial \tilde{A}}{\partial t}\right|$ has been taken.

Substitution of (3.25) and its conjugate in (3.26) gives

$$\dot{N} + \frac{N - N^e}{T_1} = \frac{-T_2}{\hbar^2} M \frac{|\mu_{12}|^2}{3} N|A|^2.$$

Using the relation $I = \frac{n\varepsilon_0 c}{2}|A|^2$ the above relation can be written as

$$\dot{N} + \frac{N - N^e}{T_1} = -\frac{|A|^2 N}{T_1 I_{sat}} \tag{3.27}$$

where I_{sat} is given by (3.22).

The instantaneous loss seen at the photon-electron interaction site is proportional to the probability of absorption. Therefore the macroscopic loss is proportional to $(N_1 - N_2)$. Similarly the macroscopic gain is proportional to $(N_2 - N_1)$. Thus, for the case of a lossy medium, (3.27) can be written as

$$\frac{\partial L(z,t)}{\partial t} + \frac{L(z,t) - L^e}{T_{1(L)}} = -\frac{|A_2|^2 L(z,t)}{T_{1(L)} I_{sat(L)}} \tag{3.28a}$$

and for a gain medium as

$$\frac{\partial G(z,t)}{\partial t} + \frac{G(z,t) - G^e}{T_{1(G)}} = -\frac{|A_1|^2 G(z,t)}{T_{1(G)} I_{sat(G)}}. \tag{3.28b}$$

The subscripts reflect the fact that the two different waveguide media may be characterized by different parameters, I_{sat} and T_1.

We have derived four partial differential equations which model the dynamic response of our proposed device where we have two coupled single-mode waveguides (one of which exhibits saturable gain and the other exhibit saturable loss). These equations governs the dynamic response of the mode amplitudes and are given as

$$\frac{\partial A_1}{\partial z} + \frac{1}{v_g} \frac{\partial A_1}{\partial t} = G A_1 + \kappa A_2, \tag{3.12}$$

$$\frac{\partial A_2}{\partial z} + \frac{1}{v_g}\frac{\partial A_2}{\partial t} = -LA_2 - \kappa A_1, \tag{3.13}$$

$$\frac{\partial L(z,t)}{\partial t} + \frac{L(z,t)-L^e}{T_{1(L)}} = -\frac{|A_2|^2 L(z,t)}{T_{1(L)}I_{sat(L)}} \tag{3.28a}$$

$$\frac{\partial G(z,t)}{\partial t} + \frac{G(z,t)-G^e}{T_{1(G)}} = -\frac{|A_1|^2 G(z,t)}{T_{1(G)}I_{sat(G)}}. \tag{3.28b}$$

The above equations can be written in a simplified dimensionless form. Assuming that

$T_{1(G)} = T_{1(L)} \equiv T_1$, $I_{sat(G)} = I_{sat(L)} \equiv I_{sat}$ and defining the following set of dimensionless

parameters:

$$a_1 = A_1/\sqrt{I_{sat}} \qquad\qquad\qquad a_2 = A_2/\sqrt{I_{sat}}$$
$$l = L/L^e \qquad\qquad\qquad\qquad g = G/G^e$$
$$y = t/T_1 \qquad\qquad\qquad\qquad x = z/(vT_1)$$
$$l_0 = v_g T_1 L^e \qquad\qquad\qquad g_0 = v_g T_1 G^e$$
$$K = \kappa v_g T_1$$

give the following dimensionless form of our differential equations

$$\frac{\partial a_1}{\partial x} + \frac{\partial a_1}{\partial y} = g_0 g a_1 + K a_2$$

$$\frac{\partial a_2}{\partial x} + \frac{\partial a_2}{\partial y} = -l_0 l a_2 - K a_1$$

$$\frac{\partial l}{\partial y} = 1 - l(1+|a_2|^2) \tag{3.29}$$

$$\frac{\partial g}{\partial y} = 1 - g(1+|a_1|^2)$$

Chapter 4

Non-Critical Point Clamping in the Steady State

The main objective of this research is to show how our proposed device clamps the mode amplitudes to a certain value (if any). This value is determined by the critical points of the system. In this chapter critical points and the phase plane are defined in general and then these definition are applied to our coupled equations (3.29). Some of the results from [6] are repeated here.

The critical point analysis and stability criteria for the case of dual saturation (where the effects of *both* loss and gain saturation are considered) is considered, as well as that for linear gain and linear loss. The main conclusion of the discussion in this chapter is that we can achieve clamping to a fixed value without waiting for convergence to a critical point to happen (hence "non-critical point clamping").

4.1   The Steady State Equations

The dimensionless parameters (a_1, a_2, l, g) in the coupled equations of (3.29) (derived in chapter 3) vary with both time and space. In the steady state these parameters become independent of time for all positions in space. Setting $\dfrac{dl}{dy} = 0$ and $\dfrac{dg}{dy} = 0$ in the loss and gain saturation equations gives the steady state loss and gain saturation equations:

$$l_{ss}(x) = \frac{1}{\{1 + [a_{2ss}(x)]^2\}}, \tag{4.1a}$$

$$g_{ss}(x) = \frac{1}{\{1+[a_{1ss}(x)]^2\}},$$ (4.1b)

and the steady state limit of the mode amplitude equations is

$$\frac{da_{1ss}(x)}{dx} = g_0 g_{ss}(x)a_{1ss}(x) + Ka_{2ss}(x),$$ (4.2a)

$$\frac{da_{2ss}(x)}{dx} = -l_0 l_{ss}(x)a_{2ss}(x) - Ka_{1ss}(x).$$ (4.2b)

Substituting (4.1) in (4.2) results in

$$\frac{da_1}{dx} = \frac{g_0}{1+a_1^2}a_1 + Ka_2,$$ (4.3a)

$$\frac{da_2}{dx} = \frac{-l_0}{1+a_2^2}a_2 - Ka_1,$$ (4.3b)

where the "ss" subscript is dropped and it will not be used since the remaining of the discussion in this chapter will refer to the steady state. Equations (4.3a) and (4.3b) are two nonlinear autonomous ordinary differential equations that describe the steady state behavior of our device.

4.2 Critical Point and Stability Analysis

Consider the following general autonomous first order system [22]

$$\frac{dx}{dt} = X(x, y), \quad \frac{dy}{dt} = Y(x, y)$$ (4.4)

this system is called autonomous since the time variable does not appear in the right-hand side of (4.4).

We may represent the solutions $x(t)$, $y(t)$ of (4.4) on a plane with Cartesian axes x, y.

When t increases, $(x(t), y(t))$ points in the plane traces out a directed curve called a *phase path* and also can be called as *a trajectory*. Assuming the following initial conditions of (4.4)

$$x = x_0, y = y_o \quad \text{at} \quad t = t_0,$$

by the existence and uniqueness theorem there is one and only solution intersecting this point when (x_0, y_0) is an "ordinary point".

The solutions of such a system describe trajectories (with t as the parameter) in a 2-dimensional phase plane which describes the phase paths.

Since $\dot{y}/\dot{x} = dy/dx$ on a path, a relevant equation is

$$\frac{dy}{dx} = \frac{Y(x, y)}{X(x, y)}. \tag{4.5}$$

The solution curves of (4.5) (the phase paths) may meet at two kinds of points. First the singular points where Y/X has some manifest singularity so that the uniqueness theorem fails. Second the critical points, of more interest here, where $X(x, y) = Y(x, y) = 0$. These critical points are also called equilibrium points and fixed points.

The direction to be associated with a trajectory can not be known from equation (4.5), but equation (4.4) can help us as follows: the signs of X and Y at a point determine the direction through the point, and generally the directions at all other points can be settled by continuity [22]. In equations (4.3a) and (4.3b) independent variable is x and the axes of the phase plane are a_1 and a_2. Plots for the phase plane of equation (4.3) will be presented later.

There are four types of trajectory behavior near the critical point, these are:

1. a center, closed paths or cycles trajectories around the critical point;

2. a saddle point, trajectories approach the critical point and then go away from it;

3. a spiral point, trajectories spiral towards (stable) or away from (unstable) the critical points; or

4. a node, trajectories are asymptotic to straight lines through the critical point moving toward (stable) or away from (unstable) the critical point.

In practice, physical and other systems are always subject to small, unpredictable variations. If such variations produce large changes in the operating conditions the system is probably unstable, and its normal operating condition would be described as unstable.

Shepard [6] has presented the critical point analysis of the steady state equations for the following different cases:

a. Dominant Loss Saturation (linear gain): the saturation of the loss is the dominant effect, i.e., $I_{sat(L)} << I_{sat(G)}$ which means that G will change very little with time and may be assumed to remain at its unperturbed value. For this case, (4.3) becomes

$$\frac{da_1}{dx} = g_0 a_1 + K a_2,$$

$$\frac{da_2}{dx} = \frac{-l_0}{1 + a_2^2} a_2 - K a_1,$$

b. Dominant Gain Saturation (linear loss): the effects of gain saturation are the dominating phenomenon, i.e., $I_{sat(L)} >> I_{sat(G)}$. For this case, (4.3) becomes

$$\frac{da_1}{dx} = \frac{g_0}{1 + a_1^2} a_1 + K a_2,$$

$$\frac{da_2}{dx} = -l_0 a_2 - K a_1.$$

c. Dual Saturation: both loss and gain saturation effects are considered.

In cases (a) and (b), there are only three real critical points (under the condition $K^2 < g_0 l_0$), whereas in case (c) there are three real and two complex critical points.

Since our interest in this thesis is the Dual Saturation case, an extended discussion of it will be presented later in this chapter. One important result of this discussion is how to avoid the complex critical points in the dual saturation.

For the second order system, linearized near the critical point, the linearized solutions are of the form

$$a_1(x) = A_1 \exp[\lambda_1 x] + B_1 \exp[\lambda_2 x],$$

$$a_2(x) = A_2 \exp[\lambda_1 x] + B_2 \exp[\lambda_2 x],$$

where A_1, B_1, A_2, B_2 are constants determined by the initial condition and λ_1, λ_2 are the eigenvalues which determine the type of the system behavior near the critical point (depending on the l_0, g_0, K parameters). If λ_1 and λ_2 are real and positive, then the critical point is an unstable node; if λ_1 and λ_2 are real and negative, then the critical point is a stable node; and if both are real but one is negative and the other is positive, then the critical point is a saddle point. If λ_1 and λ_2 are complex and the real part is negative, then the critical point is a stable spiral point; if the real part is positive, then the critical point is an unstable spiral; and if the real part is zero, then the critical point is a center.

In general, the critical points for the cases mentioned above is as follows:

Case (a): $(\dfrac{K}{g_0} a_c, -a_c)$, $(0,0)$, $(-\dfrac{K}{g_0} a_c, -a_c)$,

Case (b): $(a_c, \dfrac{-K}{l_0} a_c)$, $(0,0)$, $(-a_c, \dfrac{K}{l_0} a_c)$,

where $a_c = \left[\dfrac{g_0 l_0}{K^2} - 1 \right]^{1/2}$

25

As seen from a_c, it is needed that $K^2 < g_0 l_0$ in order to have the two real non-origin (hereafter referred to as "off-center") critical points, otherwise we will only have one critical point, the origin. In case $K^2 = g_0 l_0$, we will have only the origin as a critical point. Remember here that the axes for the phase plane are a_1, a_2.

Case (c): $\qquad\qquad (-a_{1c}, a_{2c}), \quad (0,0), \quad (a_{1c}, -a_{2c}),$

where

$$a_{1c} = \left[\left[\frac{(l_0 - g_0)g_0}{2K^2} - 1 \right] + \sqrt{ \left[\frac{(l_0 - g_0)g_0}{2K^2} - 1 \right]^2 + \frac{g_0 l_0}{K^2} - 1 } \right]^{1/2},$$

$$a_{2c} = \left[\left[\frac{(g_0 - l_0)l_0}{2K^2} - 1 \right] + \sqrt{ \left[\frac{(g_0 - l_0)l_0}{2K^2} - 1 \right]^2 + \frac{g_0 l_0}{K^2} - 1 } \right]^{1/2}.$$

The off-center critical points again exist in the real phase plane only when $K^2 < g_0 l_0$.

Detailed stability criteria for cases (a) and (b) have been presented in general in [6]. In case (c) all types of critical point behavior are possible and we can study this behavior for specific values of g_0, l_0 and K. Here we present the stability criteria of the off-center critical point for four cases that we used in this thesis.

Figures (4.1)-(4.4) shows plots of the real parts {(a) and (b)} and the imaginary parts {(c) and (d)} of the eigenvalues λ_1 and λ_2 respectively for the system with specific values of g_0, l_0 and varying K^2 for the dual saturation case when linearizing the system near the off-center critical points. In these plots K^2 is varied from 0.01 to $g_0 l_0$ so that we have three real critical points. The real part of the eigenvalue determines the stability whereas the imaginary part determines the type of the critical point (i.e., a node, a spiral, a saddle or a center).
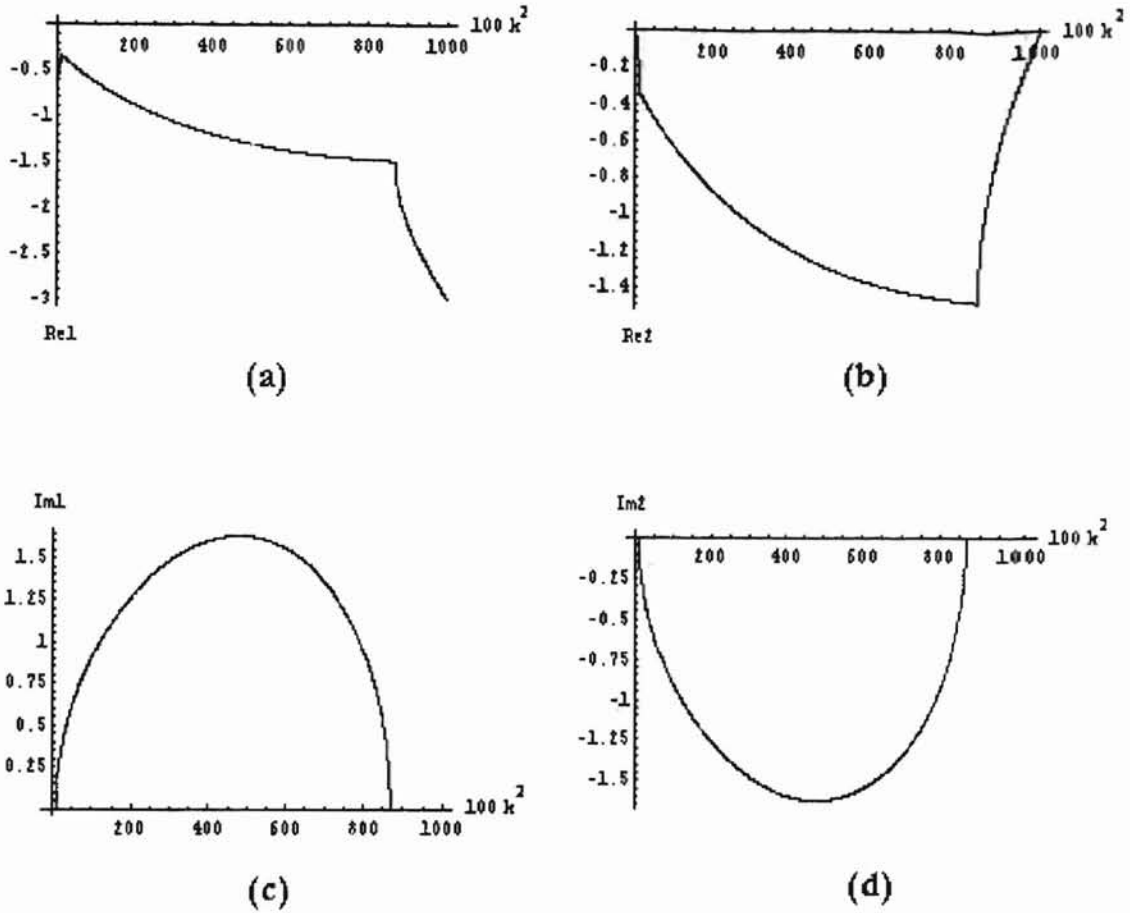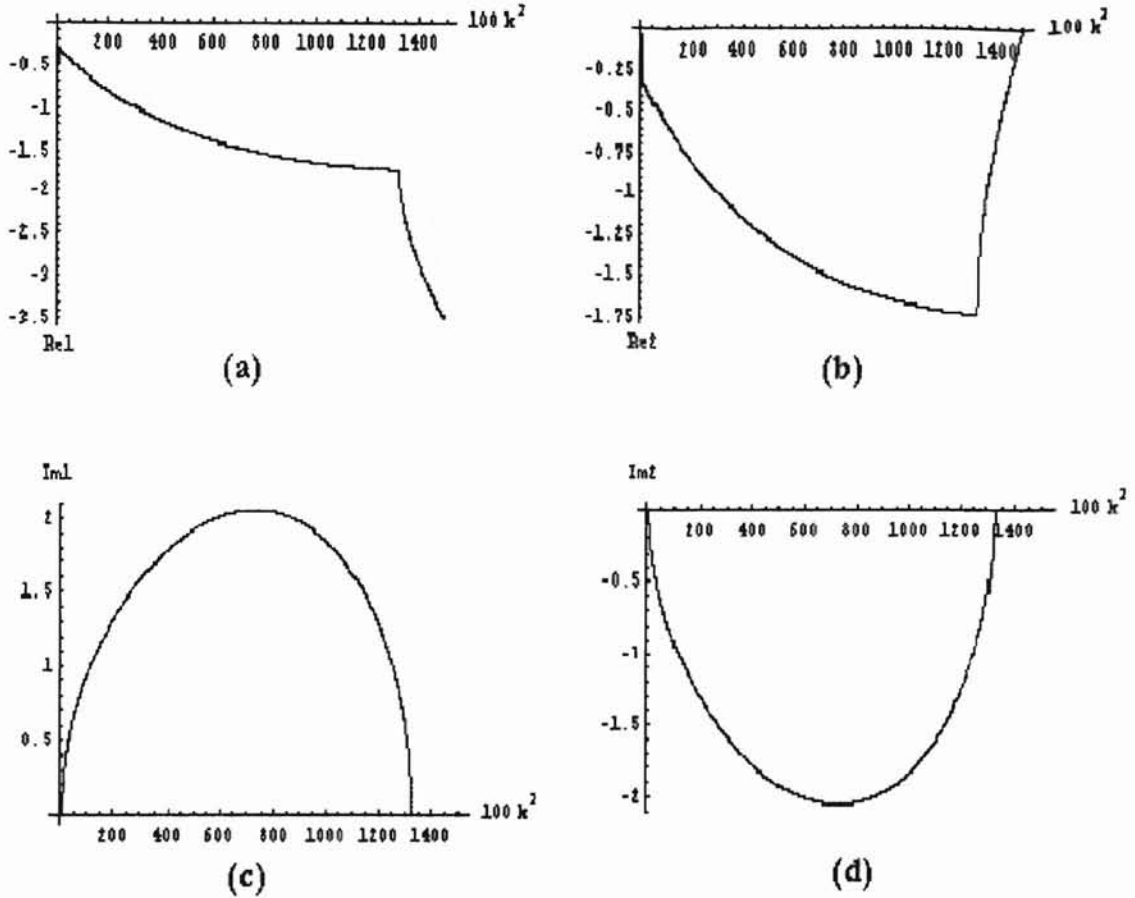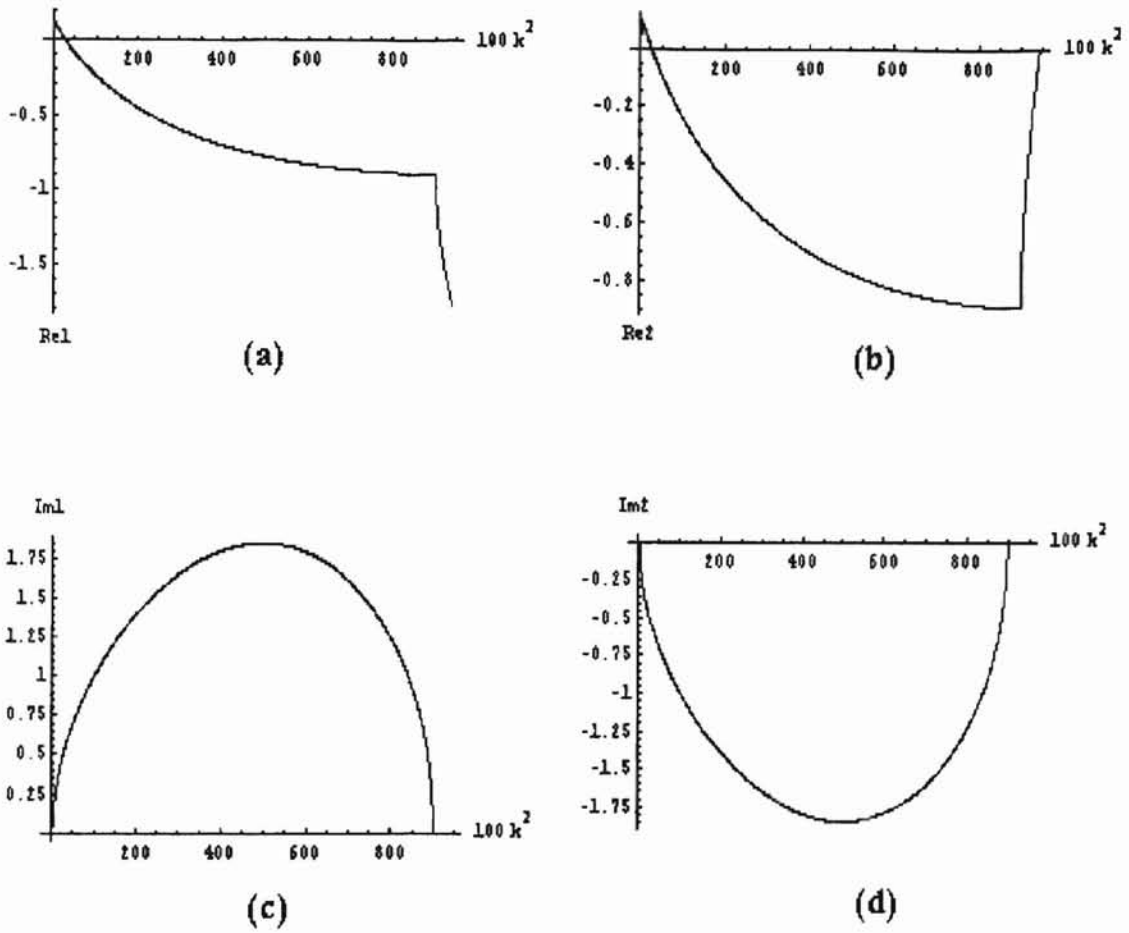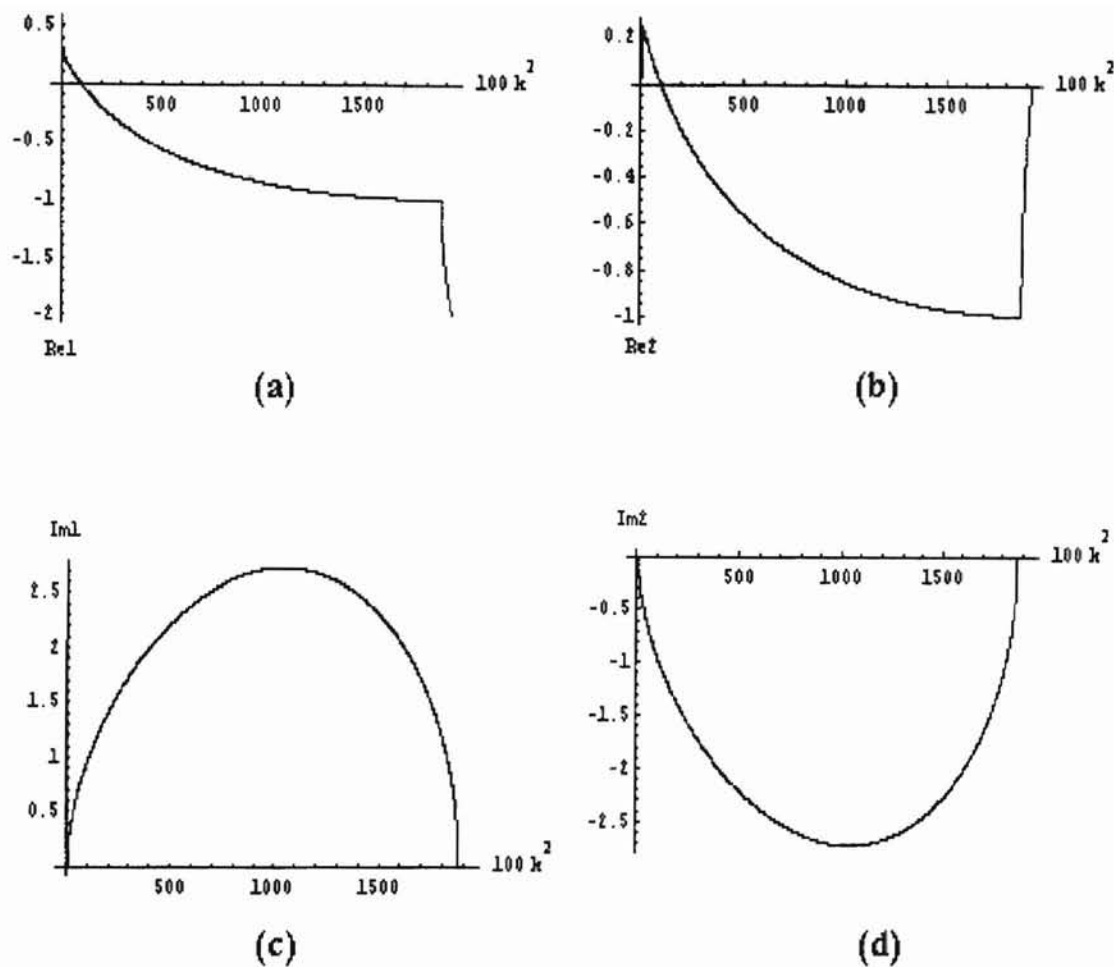
26

FIGURE 4.1: Plots of the real parts {(a) and (b)} and the imaginary parts {(c) and (d)} of the eigenvalues λ_1 and λ_2 respectively for the system with the parameters $g_0 = 2, l_0 = 5$ and variable k^2 for the dual saturation case.

FIGURE 4.2: Plots of the real parts {(a) and (b)} and the imaginary parts {(c) and (d)} of the eigenvalues λ_1 and λ_2 respectively for the system with the parameters $g_0 = 2.5, l_0 = 6$ and variable k^2 for the dual saturation case.

FIGURE 4.3: Plots of the real parts {(a) and (b)} and the imaginary parts {(c) and (d)} of the eigenvalues λ_1 and λ_2 respectively for the system with the parameters $g_0 = 2.3, l_0 = 4.1$ and variable k^2 for the dual saturation case.

FIGURE 4.4: Plots of the real parts {(a) and (b)} and the imaginary parts {(c) and (d)} of the eigenvalues λ_1 and λ_2 respectively for the system with the parameters $g_0 = 3.5, l_0 = 5.5$ and variable k^2 for the dual saturation case.

In Figure (4.1) since the real part values of both eigenvalues are negative then the system is always stable in that region where we used the parameters $g_0 = 2, l_0 = 5$. The eigenvalues are complex when K^2 is within the range 0.01-8.6869 which means the system has stable spiral off-center critical points at that range. When K^2 is larger than 8.6869 the system has stable node off-center critical points.

In Figure (4.2) the real part values of both eigenvalues are also negative and the system is always stable in that region where we used the parameters $g_0 = 2.5, l_0 = 6$. The eigenvalues are complex when K^2 is within the range 0.01-13.241 which means the system has stable spiral off-center critical points at that range. When K^2 is larger than 13.241 the system has stable node off-center critical points.

In Figure (4.3) we used the parameters $g_0 = 2.3, l_0 = 4.1$. As seen from these plots the system has unstable spiral points when K^2 is within the range 0.01-0.248 and it has stable spiral points after that till K^2 reaches the value 9.001 where the system starts to have stable node off-center critical points.

In Figure (4.4) we used the parameters $g_0 = 3.5, l_0 = 5.5$. As seen from these plots the system has unstable spiral points when K^2 is within the range 0.01-0.9532 and it has stable spiral points after that till K^2 reaches the value 18.7332 where the system starts to have stable node off-center critical points.

The above discussion proves that all types of critical point behavior are possible in the dual saturation case. Appendix (A) shows a program that can be used to generate plots similar to those in Figures (4.1)-(4.4).

Appendix (B) shows a small program to find the critical points and the eigenvalues in the case of dual saturation.

Mathematica 3.0 [24] has the ability to numerically solve some nonlinear ordinary differential equations. Figures (4.5)-(4.8) show the phase diagrams and the vector field plots for dominant loss saturation, dominant gain saturation, and dual saturation. I used different values for l_0, g_0, K so that we can see different system behaviors. The vector field plots show the direction of the trajectories in the phase plane. These figures are generated using the Mathematica program of appendix (C). A point we notice from the plots is that when the trajectory is near the critical point, it becomes very slow (the lines are each drawn for a fixed length from its initial condition).
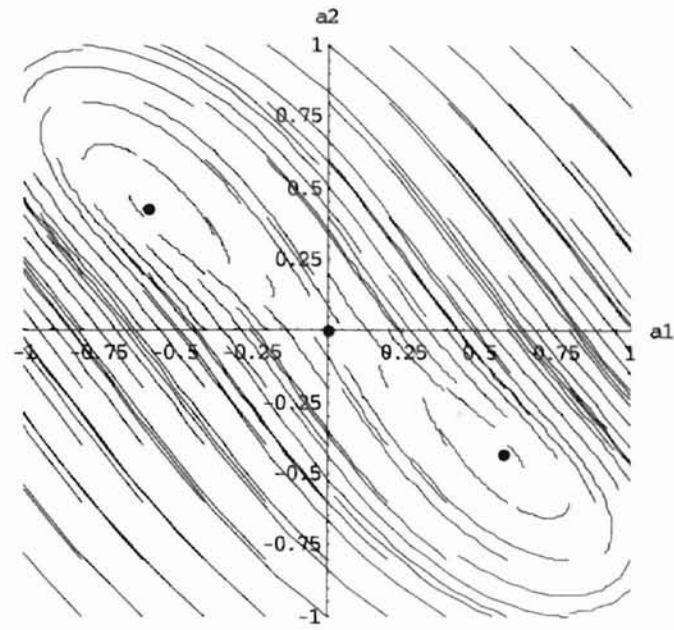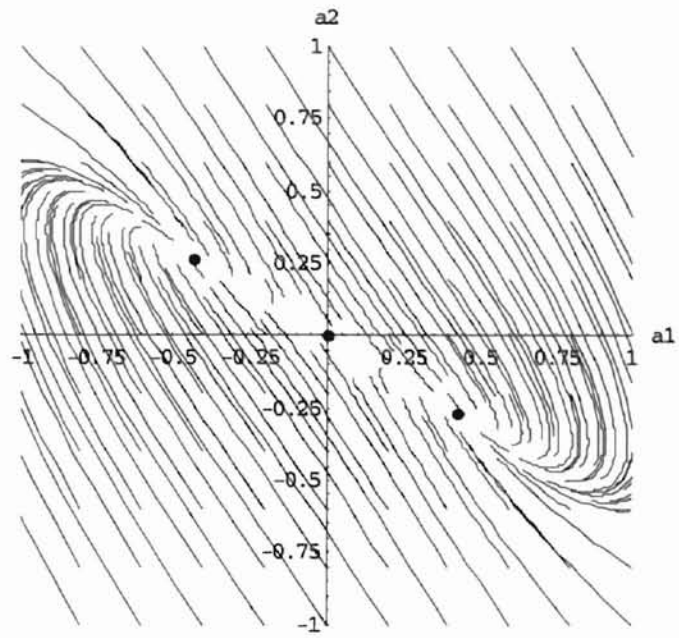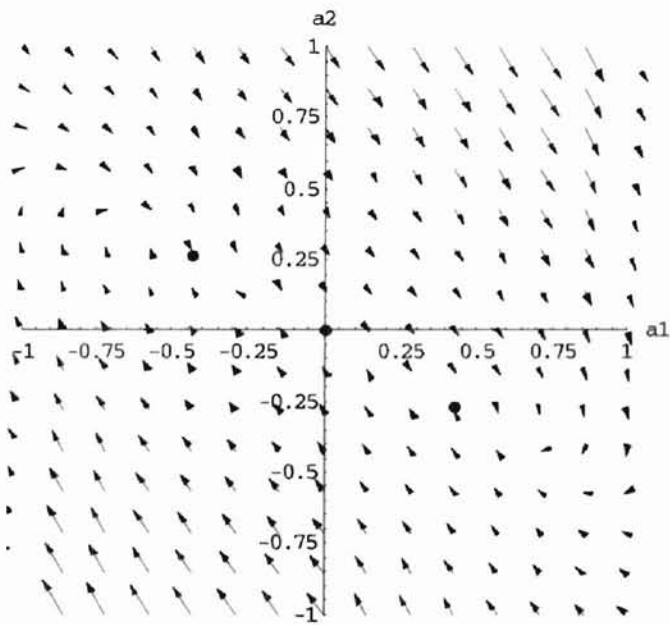
(a)
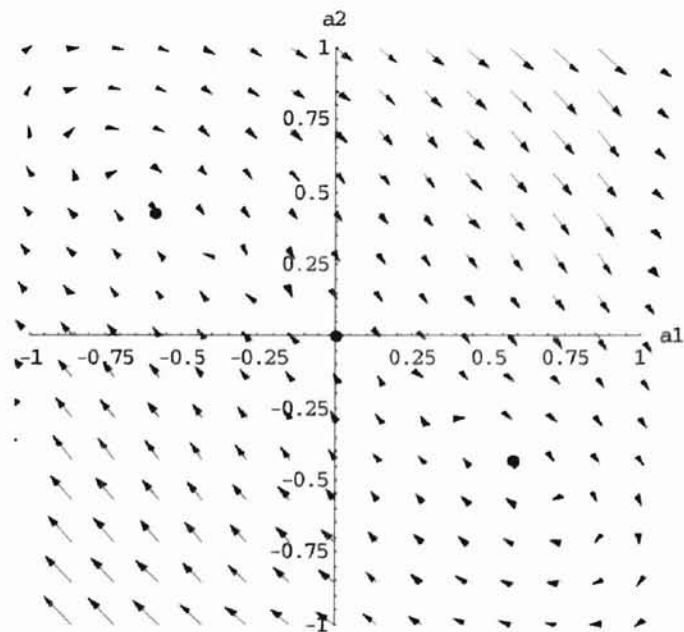
(b)

FIGURE 4.5: Phase plane (a) and vector field (b) plots for the case of dominant loss saturation where $l_0 = 5, g_0 = 2.3, K^2 = 9.695$. Each critical point is marked with a dot ($\bullet$). The off-center critical points are stable spirals and the center one is a saddle.
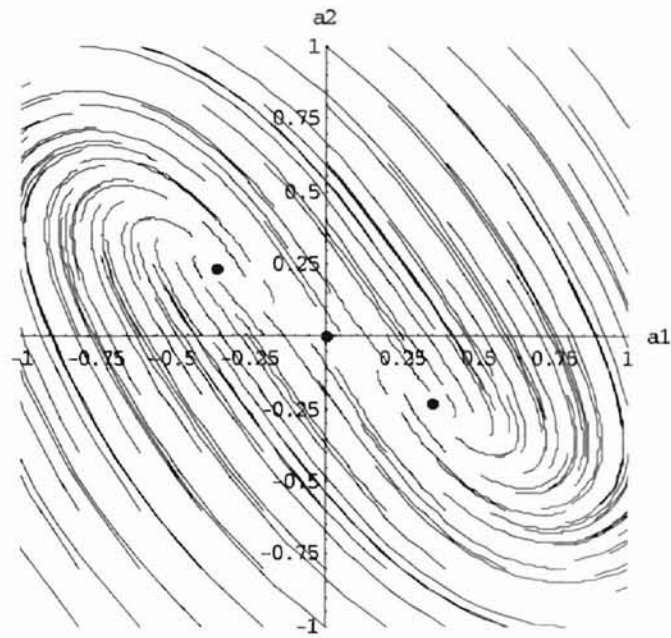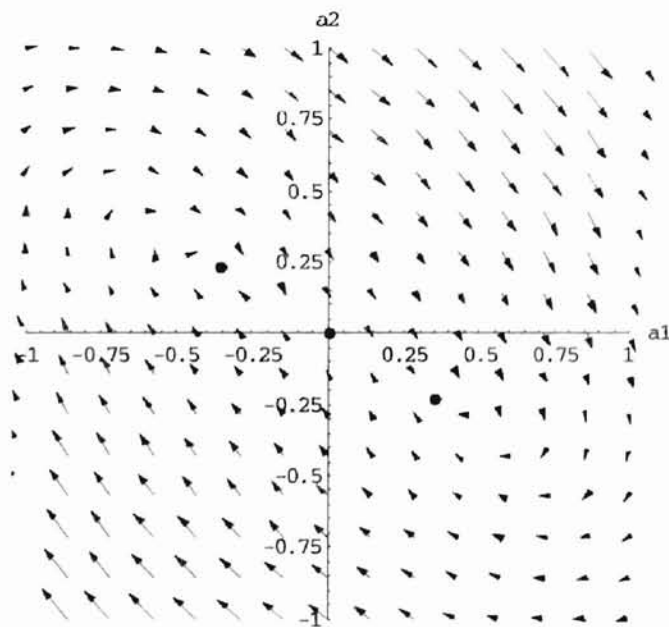
(a)

(b)

FIGURE 4.6: Phase plane (a) and vector field (b) plots for the case of dominant gain saturation $l_0 = 5, g_0 = 2.3, K^2 = 9.695$. Each critical point is marked with a dot (•). The off-center critical points are stable nodes and the center one is a saddle.
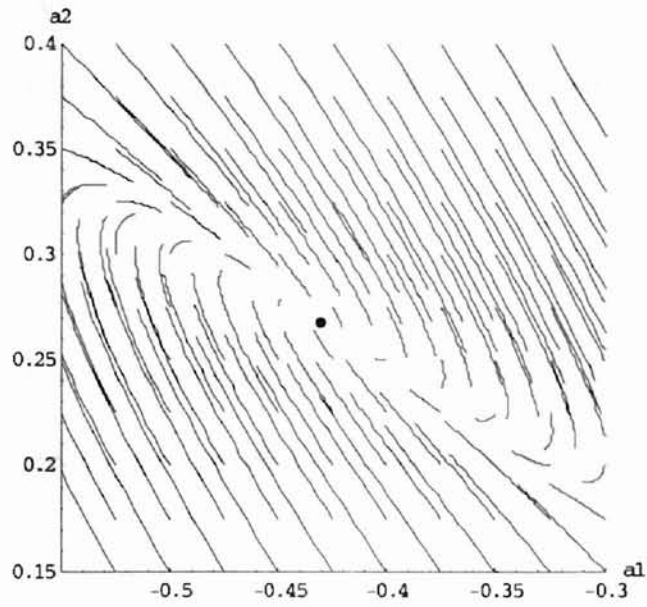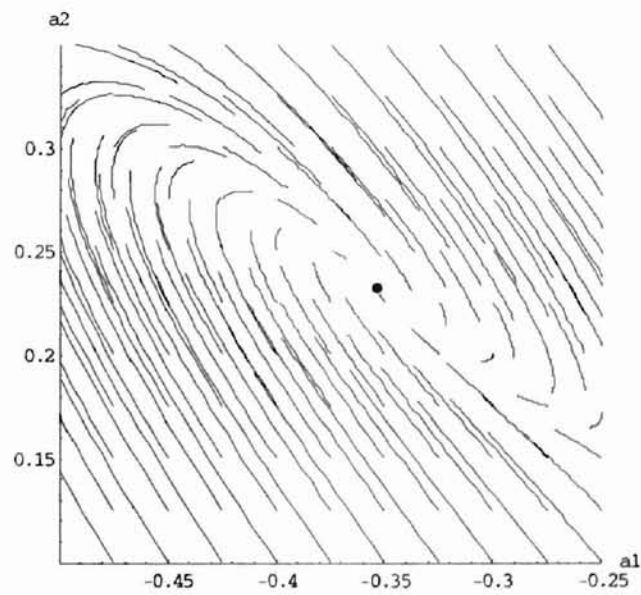
(a)

(b)

FIGURE 4.7: Phase plane (a) and vector field (b) plots for the case of dual saturation where $l_0 = 5, g_0 = 2.3, K^2 = 9.695$. Each critical point is marked with a dot ($\bullet$). The off-center critical points are a stable spiral and the center one is a saddle.

(a)

(b)

FIGURE 4.8: (a) Blow up of the phase plane near the non-origin critical point of the system presented in Figure (4.6). (b) Blow up of the phase plane near the non-origin critical point of the system presented in Figure (4.7).

4.3 Complex Critical Points Analysis for Dual Saturation

Let us return to case (c), the dual saturation, to discuss the existence of the two complex critical points. Assuming that

$$a_1 = r + js$$
$$a_2 = t + ju$$

where r, s, t, u are real numbers, then $|a_1|^2 = a_1 \cdot a_1^* = r^2 + s^2, |a_2|^2 = a_2 \cdot a_2^* = t^2 + u^2$.

Plugging the above formulae into equation (4.3) and equating the real and imaginary parts gives

$$\frac{dr}{dx} = \frac{g_0}{1+(r^2+s^2)}r + Kt$$

$$\frac{ds}{dx} = \frac{g_0}{1+(r^2+s^2)}s + Ku$$

$$\frac{dt}{dx} = \frac{-l_0}{1+(t^2+u^2)}t - Kr$$

$$\frac{du}{dx} = \frac{-l_0}{1+(t^2+u^2)}u - Ks$$

(4.6)

It turns out that the general solution of these equations for the critical point values and stability criteria is too algebraically cumbersome to be mentioned here. The general point that we do want to mention here is that these have an infinite range of critical point values that exhibit all possible stability criteria.

The main and important result we found using the numerical solution of equation (4.6), with the Mathematica program of appendix (D), is that when the initial point is $(r_0, 0, t_0, 0)$, the values of s and u stay zero all the time. In other word, real valued initial amplitudes produce trajectories that remain in the real phase plane. This result is true for all values of r_0 and t_0. The analytic proof of this result depends on the step-by-step method of finding the

37

values of r, s, t, u and on our need to stay in the real plane so that we assumed our initial condition to be $(r_0, 0, t_0, 0)$. Linearzing (4.6) by a Taylor expansion, with $(r_0, 0, t_0, 0)$ as the initial condition gives a system defined as

$$\dot{r} = \frac{g_0(1-r_0^2)}{(1+r_0^2)^2}(r-r_0) + K(t-t_0),$$

$$\dot{s} = \frac{g_0}{(1+r_0^2)}s + Ku,$$

$$\dot{t} = -K(r-r_0) - \frac{l_0(1-t_0^2)}{(1+t_0^2)^2}(t-t_0),$$

$$\dot{u} = -Ks - \frac{l_0}{(1+t_0^2)}u.$$

When deriving the above equations we noticed the following:

- The initial conditions of s and u do not appear in either $\dot{r}$ nor $\dot{t}$ equations (only because they are both assumed to be zeros). So that if s and u stay zero, then the values of r and t in the next step after which we linearize the equations will never be affected by them.

- The $\dot{r}$ equation is only coupled with the $\dot{t}$ equation, whereas the $\dot{s}$ equation is coupled only with the $\dot{u}$ equation. This simplifies the solution of the above equations.

Since we are interested in the behavior of s and u, let us assume they have the non-trivial form (i.e., A≠0, B≠0):

$s(z) = A\exp[\lambda z], u(z) = B\exp[\lambda z]$, (recall that $z \equiv$ "time" here, the independent variable).

Substituting the above solution in $\dot{s}, \dot{u}$ equations gives

38

$$(\frac{g_0}{1+r_0^2} - \lambda)A + KB = 0,$$

$$-KA - (\frac{l_0}{1+t_0^2} + \lambda)B = 0 \qquad (4.7)$$

Non-trivial solutions exist if and only if

$$\lambda^2 - (\frac{g_0}{1+r_0^2} - \frac{l_0}{1+t_0^2}) + (K^2 - \frac{g_0}{1+r_0^2}\frac{l_0}{1+t_0^2}) = 0,$$

we substitute the values of λ, found from the above equation, in (4.7) to find the corresponding values for A and B. Fortunately, the only values we get for A and B are zeros.

Thus we have analytic confirmation that real amplitudes remain real. Figure (4.9) shows plots for $r(z), s(z), t(z), u(z)$ generated by numerically solving (4.6) for the parameters $l_0 = 5, g_0 = 2, K^2 = 8.505$, and the initial conditions $r_0 = 1, s_0 = 0, t_0 = 2, u_0 = 0$. As shown in these plots, s and u stay at their initial conditions. In Figure (4.10) we used the same parameters and the same initial conditions for r, t, u but we now used 0.1 as the initial condition for s. This small deviation from zero for s_0 causes s and u to have values other than zero in the phase plane, which means that we have complex values for a_1 and a_2. Also we can notice how $r(z), s(z), t(z), u(z)$ are clamped to the critical point.

Physically, this result that real amplitudes remain real, simply means that the electrical fields (corresponding to a_1 and a_2) do not incur any extra phase shifts.
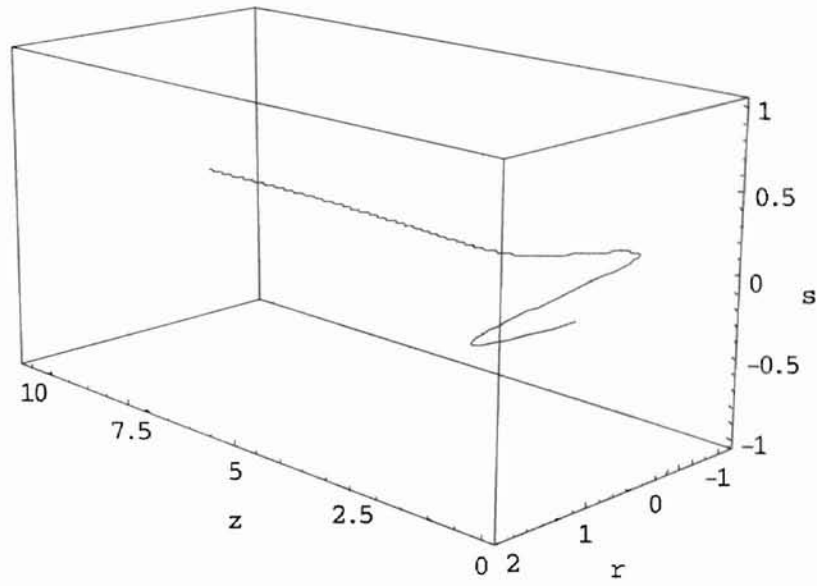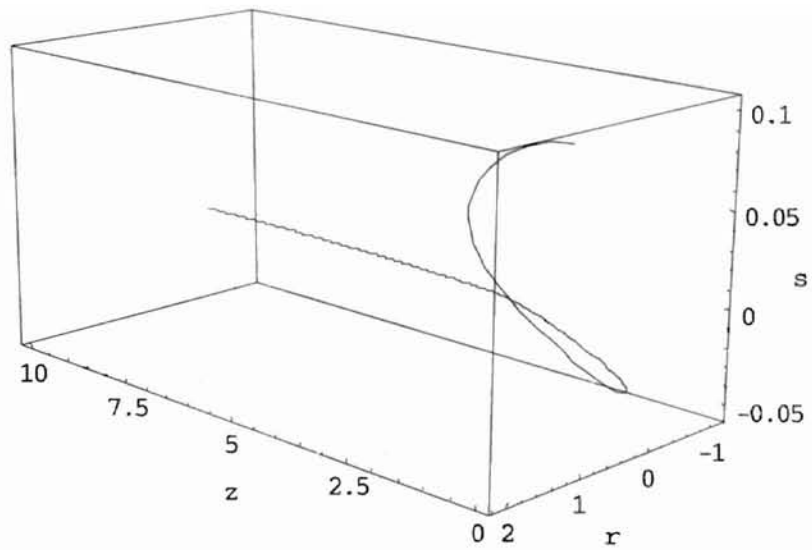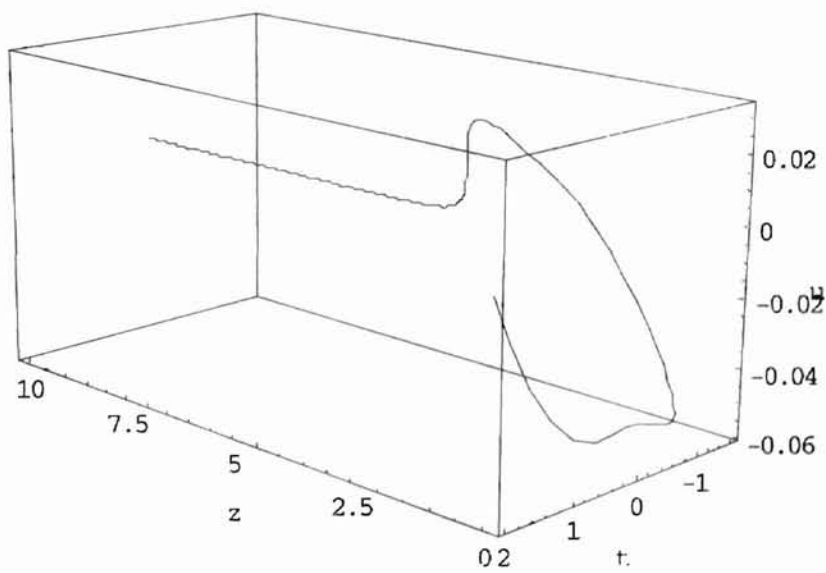
(a)
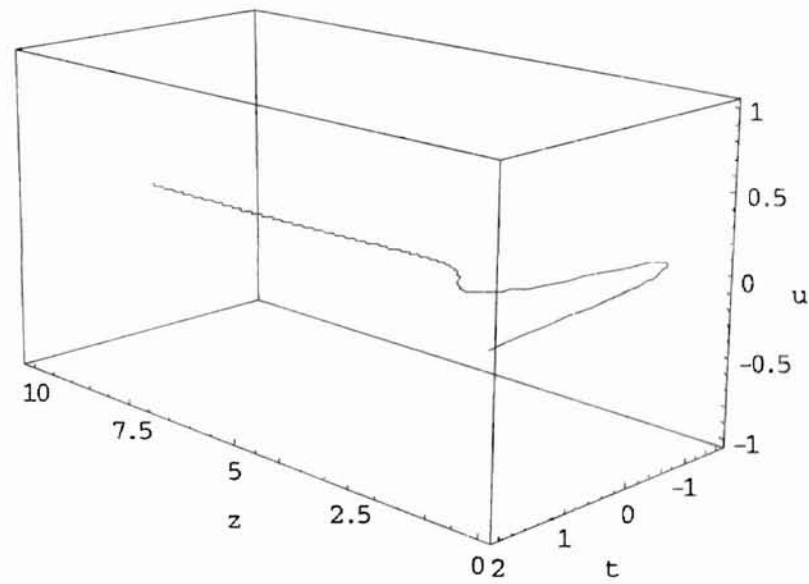
(b)

FIGURE 4.9: Plots for $\{r(z), s(z)\}(a), \{t(z), u(z)\}(b)$ generated by numerically solving equations (4.6) for the parameters $l_0 = 5, g_0 = 2, K^2 = 8.505$, and the initial conditions $r_0 = 1, s_0 = 0, t_0 = 2, u_0 = 0$.

(a)

(b)

FIGURE 4.10: Plots for $\{r(z), s(z)\}(a), \{t(z), u(z)\}(b)$ generated by numerically solving

equations (4.6) for the parameters $l_0 = 5, g_0 = 2, K^2 = 8.505$, and the initial conditions

$r_0 = 1, s_0 = 0.1, t_0 = 2, u_0 = 0$.

4.4 Non-Critical Point Clamping

The relevancy of the critical point analysis is to show to what values (if any) a_1 and a_2 will be clamped to. These values determine the physical parameters and dimensions of our device.

A key question here (regarding the manufacturability of a usable device) is "do we need really to wait for a_1 and a_2 to reach the critical point?" The surprising and very useful answer is "No!" Figures (4.11) –(4.14) show a major improvement on the concept of clamping to the critical point. In these plots we clamped a range of amplitudes of the input signal to a certain value which is not necessarily the critical point of the system. These plots are generated for the case of dual saturation. This clamping is achieved with smaller lengths than what is really needed to reach the critical point.

Figure (4.11a) is generated using the program of appendix (E), Figures (4.11b), (4.12), (4.13) and (4.14) are generated using the program of appendix (F) but with changing the parameters, the range of the input signal and the length to suit each case. The programs of appendices (E) and (F) are written with Mathematica software package.

Figure (4.11) shows the non-critical point clamping for a system with the following parameters $g_0 = 5, l_0 = 6, K^2 = 6.9$. In this figure, the a_1 input signal range is (-1.1 to -1.7) and it is clamped to $a_1 = -1.583$ with a length $x = 0.654$. Plot (a) in this figure shows the trajectories, whereas plot (b) shows only the final values for a_1 and a_2, i.e., $(a_1(0.654), a_2(0.654))$. Figure (4.12) shows the non-critical point clamping for a system with the following parameters $g_0 = 3, l_0 = 3.01, K = 5.9$. In this figure, the a_1 input signal range is (-1.4 to -2.0) and it is clamped to $a_1 = -1.078$ with a length $x = 0.637$. In this figure we show only the plot of the final values for a_1 and a_2, i.e., $(a_1(0.637), a_2(0.637))$.

Figure (4.13) shows the non-critical point clamping for a system with the following

parameters $g_0 = 3, l_0 = 4.5, K^2 = 7.9$. In this figure, the a_1 input signal range is (-1.2 to -1.8)

and it is clamped to $a_1 = -1.027$ with a length $x = 0.592$. In this figure we show only the

plot of the final values for a_1 and a_2, i.e., $(a_1(0.592), a_2(0.592))$. We used different

parameters to show that the non-critical point clamping can be achieved for different values

giving different required results. In Figures (4.11)-(4.13) we clamped a_1, whereas in Figure

(4.14) we show that it is also possible that a_2 could be clamped to a certain value. This

figure is generated using $g_0 = 3.5, l_0 = 5.5, K^2 = 5$. In this figure, the a_1 input signal range

is (-1.6 to –2.0) and a_2 is clamped to 1.05 with a length $x = 1.49$. In all figures generated the

initial value of a_2 is always zero and the off-center critical points are stable spiral points.
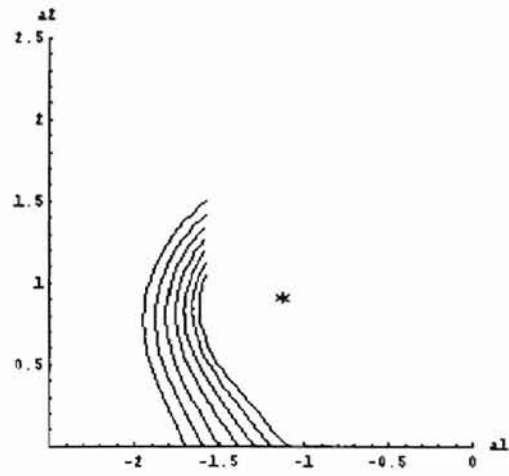
(a)
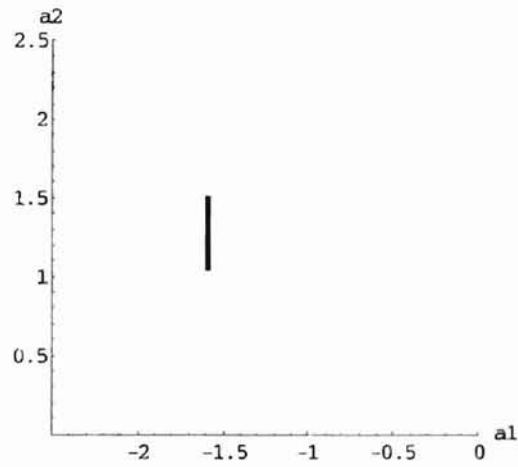
(b)

FIGURE 4.11: Trajectory plot (a) and the final values of the trajectories (b) of the system with the parameters $g_0 = 5, l_0 = 6, K^2 = 6.9$ and $x = 0.654$. The critical point marked with a (*) is a stable spiral point. The initial value of a_1 has the range (-1.1 to -1.7) and the initial value of a_2 is zero.
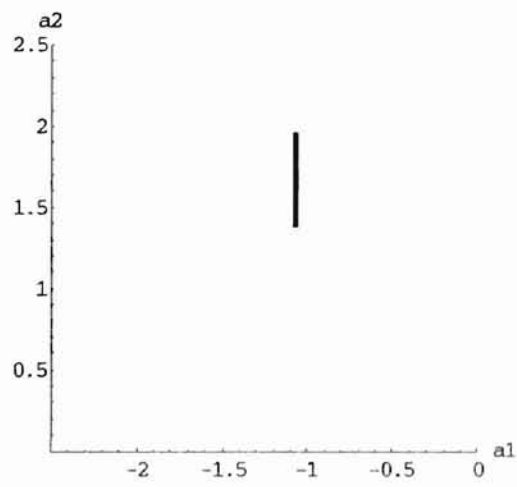
FIGURE 4.12: The final values of the trajectories of the system with the parameters $g_0 = 3, l_0 = 3.01, K^2 = 5.9$ and $x = 0.637$. The off-center critical points are stable spirals. The initial value of a_1 has the range (-1.4 to –2.0) and the initial value of a_2 is zero.
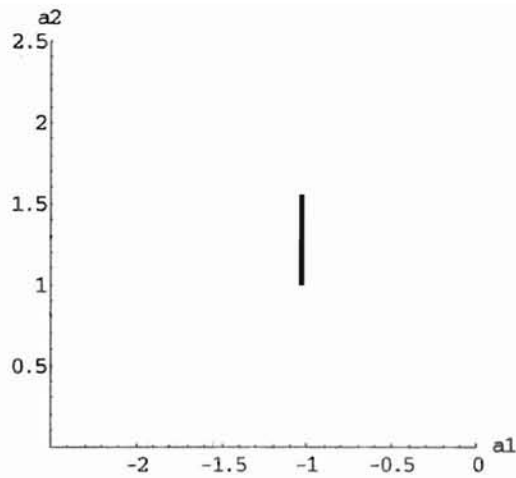
FIGURE 4.13: The final values of the trajectories of the system with the parameters $g_0 = 3, l_0 = 4.5, K^2 = 7.9$ and $x = 0.592$. The off-center critical points are stable spirals. The initial value of a_1 has the range (-1.2 to -1.8) and the initial value of a_2 is zero.
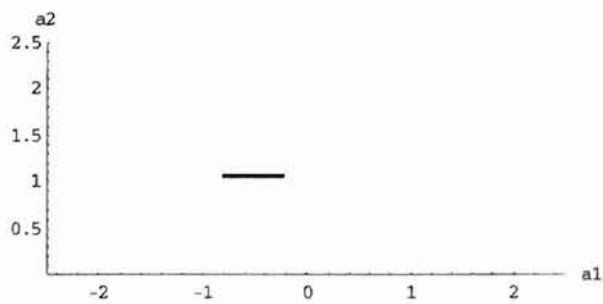

FIGURE 4.14: The final values of the trajectories of the system with the parameters $g_0 = 3.5, l_0 = 5.5, K^2 = 5$ and $x = 1.49$. The off-center critical points are stable spirals. The initial value of a_1 has the range (-1.6 to -2.0) and the initial value of a_2 is zero.

DYNAMIC RESPONSE for DUAL SATURATION

In this chapter we discuss the dynamic response of our proposed device when arbitrary input excitations are used.

In the first section we will give a reasonable mathematical and physical explanation of why we need to consider the case of dual saturation. In the second section the pulse frame transformation and the numerical scheme for solving the equations in (3.29) for the dual saturation case are briefly presented. Based on the quantized form of the equations in (3.29), a simulation program is written with Mathematica 3.0. Results from excitation by two different waveshapes for various heights and widths are presented in the third section for different device parameterizations. To understand how this proposed device works, physical interpretations of the results are offered in the last section.

5.1 Why Dual Saturation?

The coupled equations (3.29) are nonlinear since they involve $|a_1|^2$ and $|a_2|^2$ where a_1 and a_2 are the mode amplitudes normalized to $I_{sat(G)}$ and $I_{sat(L)}$ respectively. If I_{sat} is so large for either L or G, then L or G will change very little with time and may be assumed to remain at its unperturbed value.

Let us assume that $I_{sat(G)}$ is so large, then

$$\frac{\partial g}{\partial y} = 0 \Rightarrow g = \frac{1}{1+|a_1|^2} \text{, but } |a_1|^2 \text{ is so small compared to 1 so this gives } g = 1 \text{ and we}$$

will have

$$\frac{\partial a_1}{\partial x} + \frac{\partial a_1}{\partial y} = g_0 a_1 + K a_2,$$

which means that the gain saturation has no effect (i.e., we neglect the gain saturation) and the system works in the linear gain region.

When linearizing the coupled equations by assuming that $A \ll \sqrt{I_{sat}}$, $K^2 \to^{(-)} g_0 l_0$ for the case of stable critical point. But as $K^2 \to^{(-)} g_0 l_0$, $a_c = \sqrt{\frac{g_0 l_0}{K^2} - 1}$ will approach zero. This means that we still have stable critical points even if they are very close to zero. From this we learn that we can not always linearize the gain and loss effects and the dual saturation case is needed.

Linearizing the gain or the loss requires building our device with two different values of the saturation intensity implying that we use two different materials for the waveguides. But when this happens, we have to look to the other parameters T_1 and v_g which depend on the materials of the waveguides. Designing the device with different materials changes our coupled equations, unless we assume certain approximations like $T_{1(G)} = T_{1(L)}$ and $v_{g(G)} = v_{g(L)}$.

In this thesis we will use the above assumption as a start but we will add a new variable $f \equiv I_{sat(G)} / I_{sat(L)}$. This new variable will give an indication of small or big is our gain saturation intensity compared to the loss saturation intensity, i.e., the coupled equations will be written as

48

$$\frac{da_1}{dx} = \frac{g_0}{1 + (a_1^2 / f)} a_1 + Ka_2,$$

$$\frac{da_2}{dx} = \frac{-l_0}{1 + a_2^2} a_2 - Ka_1,$$

Then when $f \to \infty$, we will get the linear gain case. Thus f will affect the location of the critical points and the stability criteria as expected.

By studying the dynamic response we will prove that the case when $f = 1$ (i.e., $I_{sat(G)} = I_{sat(L)}$, a practical case that helps us to fabricate our device with similar materials for the waveguides) we observe improved behavior.

5.2 Numerical Solution of the Mathematical Model

Most of the physics and engineering problems fall naturally into one of the following physical categories: equilibrium problems, eigenvalue problems, and propagation problems [24]. Our problem in this thesis can be categorized as a propagation problem which in mathematical parlance is known as initial boundary value problem. The governing equation of any problem can be classified using the concept of characteristics. Using this concept the propagation problems are parabolic or hyperbolic. Our mathematical model governed by the coupled equations in (3.29) may be classified as a parabolic system that has one characteristic direction along the lines $y = x + b$ where y is the dimensionless time variable (normalized to T_1), x is the dimensionless space variable (normalized to $v_g T_1$), and b is the y intercept.

The coupled equations in (3.29) have two basic directions of propagation:

- the y direction along which the loss and gain saturate,

49

- the characteristic direction (i.e., the lines $y = x + b$) along which the mode amplitudes propagate.

Based on the above discussion, Shepard [6] used what he referred to as pulse frame transformation that results in a significant reduction of mathematical complexity and computational difficulty. In this transformation we assume that

$$x = x(s) = s; \ y = y(s) = s + b, \ \text{(see Figure (5.1))}$$

then $\dfrac{\partial}{\partial s} = \dfrac{\partial}{\partial x} + \dfrac{\partial}{\partial y}$ and

$$g(x, y) = g(s, y), a_1(x, y) = a_1(s, y), l(x, y) = l(s, y), a_2(x, y) = a_2(s, y).$$

Therefore, the coupled equations in (3.29) can be written as:

$$\frac{\partial a_1(s, y)}{\partial s} = g_0 g(s, y) a_1(s, y) + K a_2(s, y), \tag{5.1a}$$

$$\frac{\partial a_2(s, y)}{\partial s} = -l_0 l(s, y) a_2(s, y) - K a_1(s, y), \tag{5.1b}$$

$$\frac{\partial l(s, y)}{\partial s} = 1 - l(s, y)[1 + (a_2(s, y))^2], \tag{5.1c}$$

$$\frac{\partial g(s, y)}{\partial s} = 1 - g(s, y)[1 + (a_1(s, y))^2 / f]. \tag{5.1d}$$

The pulse frame transformation results in substantial simplification since equation (5.1) has derivatives with respect to one independent variable only.

Shepard [6] has presented a detail discussion of the problems of convergence, stability, and computation time, which arise when choosing a quantization scheme for the numerical solution of a differential equation. Here we will not present this discussion and we will only adopt his choice of choosing two different finite difference schemes. These are a third order

50

backward difference scheme for the time (y) derivatives and a first order backward difference formula for the derivatives with respect to (s).

The use of these schemes results in the following quantization of the dynamic equations for the dual saturation case (that is the case we are interested in here):

$$a_{1(i,j)} - a_{1(i-1,j)} - (\delta s)g_0 g_{(i,j)} a_{1(i,j)} - (\delta s)Ka_{2(i,j)} = 0, \tag{5.2a}$$

$$a_{2(i,j)} - a_{21(i-1,j)} + (\delta s)l_0 l_{(i,j)} a_{21(i,j)} + (\delta s)Ka_{1(i,j)} = 0, \tag{5.2b}$$

$$11g_{(i,j)} - 18g_{(i,j-1)} + 9g_{(i,j-2)} - 2g_{(i,j-3)} + 6(\delta y)g_{(i,j)}[1 + (a_{1(i,j)})^2 / f] - 6(\delta y) = 0, \tag{5.2c}$$

$$11l_{(i,j)} - 18l_{(i,j-1)} + 9l_{(i,j-2)} - 2l_{(i,j-3)} + 6(\delta y)l_{(i,j)}[1 + (a_{2(i,j)})^2] - 6(\delta y) = 0, \tag{5.2d}$$

where δy and δs are the step length on y and s axes respectively.

The main results of the discussion of the convergence and stability of the above numerical scheme devised by Shepard [6] are:

a- $\left|\varepsilon_j^{(l)}\right| \leq |E|$, where $\varepsilon_j^{(l)}$ represents the total quantization error for l at that point and

$|E|$ is some maximum error, hence the scheme is "stochastically stable."

b- $(\delta s) < (1/g_0)$. Equation (5.2) is proven to be non-convergent when this condition is

violated.

In solving the equations in (5.2) we assume an input pulse, say $pulse(y)$, is fed into the gain medium waveguide while the lossy waveguide input is kept at zero. We assume that the system is initially unperturbed, the initial boundary conditions are:

$$a_1(x,0) = 0, a_2(x,0) = 0, l(x,0) = 1,$$
$$a_1(0, y) = pulse(y), a_2(0, y) = 0, l(0, y) = 1,$$

and all previous condition were unperturbed also, i.e.,

$$l_{(i,0)} = l_{(i,-1)} = l_{(i,-2)} = 1, \quad g_{(i,0)} = g_{(i,-1)} = g_{(i,-2)} = 1.$$

Figure (5.1) shows how we numerically integrate the equation (5.2) to find the value of a_1 at

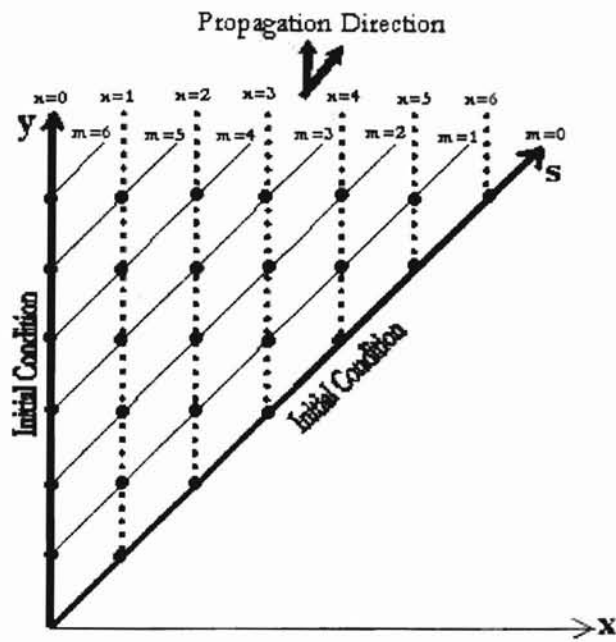all the points in the propagation (space-time) diagram.

FIGURE 5.1: The propagation (space-time) diagram used to integrate equations (5.2) numerically. The (●) represents the (n,m) steps where n ≡steps in space and m ≡steps in time.

5.3 Dynamic Response Results and Interpretations

In this section certain results for the dynamic response of different cases will be represented. These results are generated using the Mathematica simulation program of appendix [G] which gives the shape of the pulse at any point along the waveguides. Our plots will represent the shapes of a_1 that propagate along the gain waveguide (the waveguide with pump).

Two different pulse types are considered here as the initial value (injected pulse in the gain waveguide). The first one is a logic pulse defined as:

$$P_0(y) = \begin{cases} A[1 - \exp(-y/\tau) & 0 \le y \le 4\tau \\ A[1 - \exp(-4)] & 4\tau \le y \le 8\tau \\ A[1 - \exp((y - 12\tau)/\tau)] & 8\tau \le y \le 12\tau \end{cases},$$

where

$A \equiv$ the pulse amplitude,

$\tau \equiv$ a normalized time constant that determines the rising/dropping time of the leading/trailing edge and in the above pulse it also determines the pulse width.

The second input pulse to be considered here is the hyperbolic secant pulse. This pulse shape is close to the ones used in fiber optic communication systems and also is known to be a soliton for various media. The pulse is defined as:

$$P_0(y) = A \cdot Sech[0.8844(y - 6\tau)/\tau],$$

where

$A \equiv$ the pulse amplitude,

and 2τ is the pulse full width at half maximum (FWHM).

The plots presented here are for the normalized pulse amplitude, a_1, versus normalized time, y, at four different values of normalized distance, x. These distances are at steps

54

$i = 2,4,8,16$ when using a logic pulse as the input and $i = 4,8,12,18,24$ when using a hyperbolic secant pulse as the input. Using $\delta s = 0.4$ these steps correspond to $x = \dfrac{\delta s}{\sqrt{2}} i$.

Three-dimension (3-D) plots for the pulse amplitude, a_1, propagating through the waveguide will be given for some cases.

Figure (5.2) shows a plot that represents the difference between the value of a_1 at the critical point for the case of linear gain and the case of dual saturation for various f. This plot is generated using the program of appendix (H) to determine if for large values of f (and then how large) the dual saturation case results will resemble those predicted by the dominant loss saturation equations. Figure (5.2) is generated using the parameters $g_0 = 2, l_0 = 5, K^2 = 8.505$. From this figure we see that when $f \geq 15$ the difference between the value of a_1 at the critical point for the case of linear gain and the case of dual saturation is ≤ 0.038. So the case when $f = 15$ is a reasonable choice where the dual saturation case results will resemble those predicted by the dominant loss saturation equations.

The results of the dynamic response when using the logic pulse input are presented in three groups of plots. In the first group we study the response of the system when changing the value of f. The values of f used in Figure (5.3) are 1 in (5.3a), 5 in (5.3b), and 15 in (5.3c). This group of plots is generated using the parameters $g_0 = 2, l_0 = 5, K^2 = 8.505, \tau = 4, A = 0.2$. From Figure (5.3) we notice that the overshoot experienced by the leading edge is less for the case when $f = 1$. This makes $f = 1$ (dual saturation case) a good choice when building our device. All of the remaining plots are generated using $f = 1$.
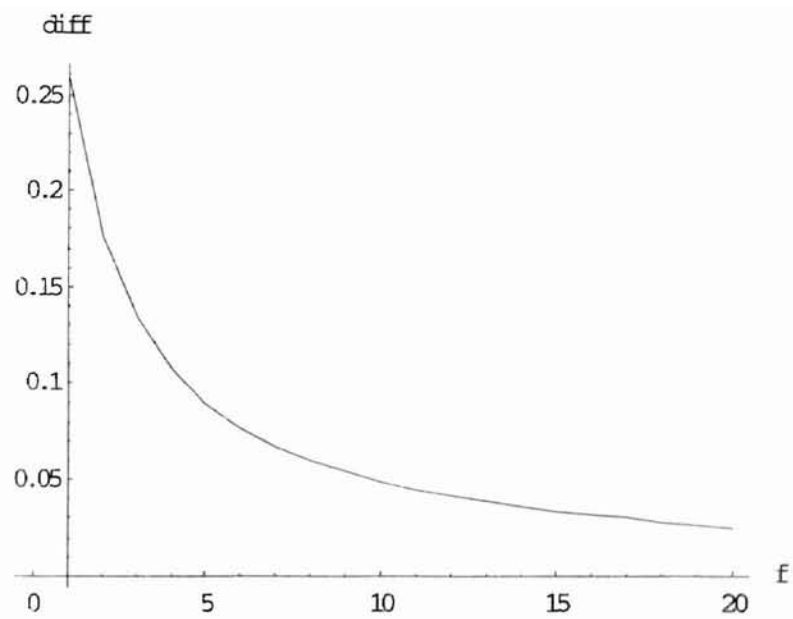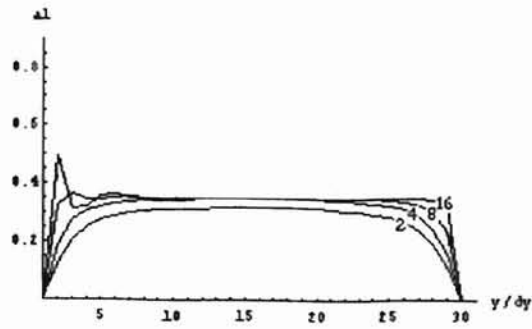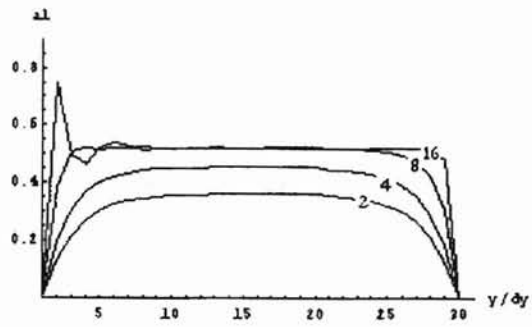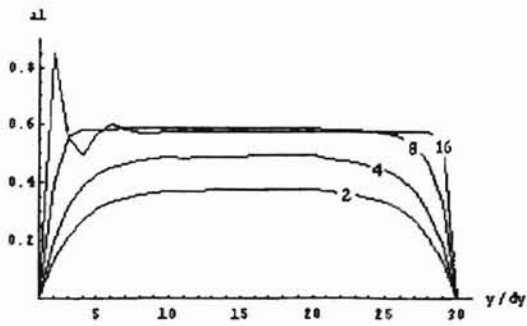
FIGURE 5.2: The difference between the value of a_1 at the critical point for the case of linear gain and the case of dual saturation for variable f.
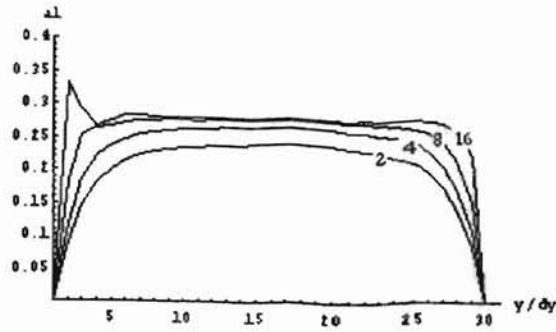
(a)

(b)

(c)

FIGURE 5.3: Device dynamic response for a logic pulse input at the labeled positions with

$f = 1$ in (a), 5 in (b), and 15 in (c). The parameters used are

$g_0 = 2, l_0 = 5, K^2 = 8.505, \tau = 4, A = 0.2$.

In the second group, Figure (5.4), we vary the amplitude of the input pulse in an attempt to show how the overshoot (or ringing) varies with different input amplitudes (all less and near the critical point value, which in this case is at $a_1 = 0.28$). The plots where generated using the parameters $g_0 = 2, l_0 = 5, K^2 = 9.0, \tau = 4$. In Figure (5.4a) the input amplitude is 0.15, in Figure (5.4b) it is 0.2 and in Figure (5.4c) it is 0.25. We observe in Figure (5.4) that the overshoot increases slightly as the amplitude increases. Since the device must operate over a range of input pulse amplitudes, we need to find some other way to decrease the overshoot.

The third group is generated in an attempt to reduce this problem by altering K^2. In generating the plots in Figure (5.5) we used the parameters $g_0 = 2, l_0 = 5, A = 0.15, \tau = 4$ and the value of K^2 is 9.0 in Figure (5.5a), 9.2 in Figure (5.5b) and 9.4 in Figure (5.5c). All the cases in this group have stable node critical points. These plots show that the overshoot decreases with increasing the coupling coefficient. Perhaps this is because the device reaches the critical point faster when the coupling coefficient is higher.

The more interesting and practical results are when injecting the device with hyperbolic secant pulses. For this pulse shape we generated two groups. The first is in Figure (5.6) where we changed the coupling coefficient with fixing the other parameters as follows $g_0 = 2.3, l_0 = 4.1, A = 0.18, \tau = 4$. The value of K^2 is 8.305 in Figure (5.6a), 8.505 in Figure (5.6b) and 8.705 in Figure (5.6c). All the cases in this group have stable spiral critical points. As seen from the 3-D plot, Figure (5.7), for the larger overshoot case of Figure (5.6a), the pulse starts to be amplified in its first steps in the device. After that the leading edge starts to feel the effect of the critical point and it starts to steepen up while experiencing

(a)
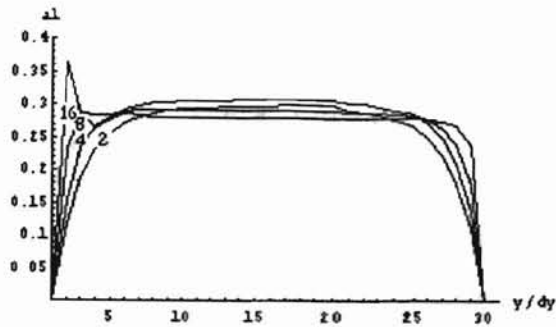
(b)
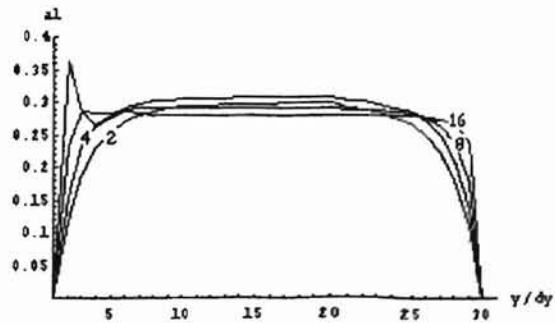
(c)

FIGURE 5.4: Device dynamic response for a logic pulse input at the labeled positions with varying input pulse amplitude which is 0.15 in (a), 0.2 in (b), and 0.25 in (c). The parameters used are $g_0 = 2, l_0 = 5, K^2 = 9.0, \tau = 4$.

59
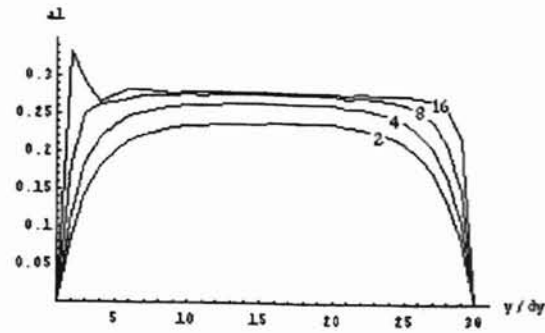
FIGURE 5.5: Device dynamic response for a logic pulse input at the labeled positions with varying K^2 as 9.0 in (a), 9.2 in (b), and 9.4 in (c). The parameters used are $g_0 = 2, l_0 = 5, A = 0.15, \tau = 4$.
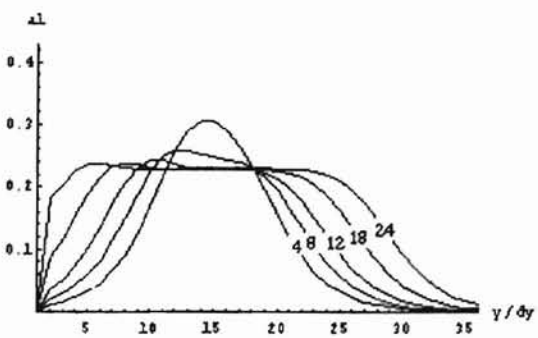
FIGURE 5.6: Device dynamic response for a secant hyperbolic pulse input at the labeled

positions with varying K^2 as 8.305 in (a), 8.505 in (b), and 8.705 in (c). The parameters used

are $g_0 = 2.3, l_0 = 4.1, A = 0.18, \tau = 4$.

FIGURE 5.7: The pulse propagation in the device for the case of a secant hyperbolic pulse

input where K^2 is 8.305 and $g_0 = 2.3, l_0 = 4.1, A = 0.18, \tau = 4$.

an overshoot. The main result from these plots in Figure (5.6) is that the overshoot is less when increasing the coupling coefficient (as we also observed, in Figure (5.5), for the logic pulse). The third group of plots is generated for different input amplitudes while fixing the other parameters as $g_0 = 2.3, l_0 = 4.1, K^2 = 8.605, \tau = 4$. The input amplitudes used are 0.18 in Figure (5.8a), 0.2 in Figure (5.8b) and 0.22 in Figure (5.8c). These plots are generated to show how the device responds over a range of input amplitudes. A 3-D plot for the case used in Figure (5.8c) is shown in Figure (5.9).
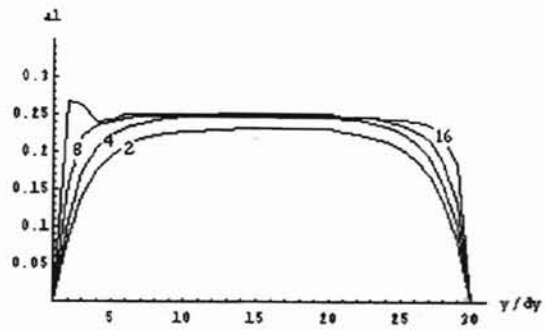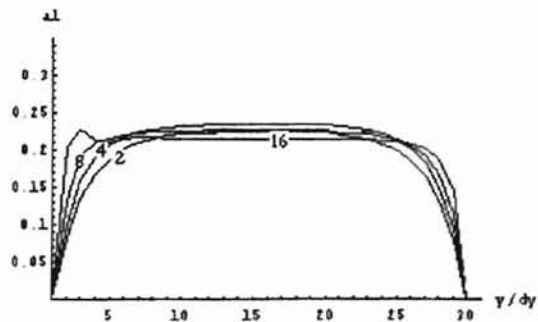
FIGURE 5.8: Device dynamic response for a secant hyperbolic pulse input at the labeled positions with varying the amplitude as 0.18 in (a), 0.2 in (b), and 0.22 in (c). The parameters used are $g_0 = 2.3, l_0 = 4.1, K^2 = 8.605, \tau = 4$.
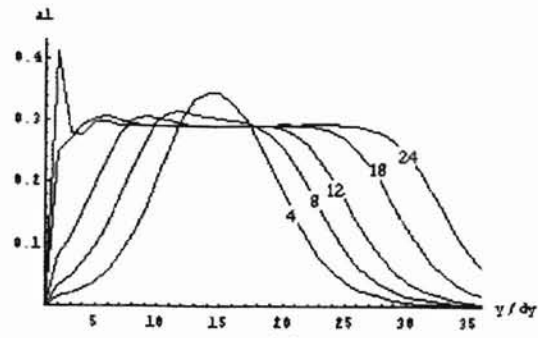
64

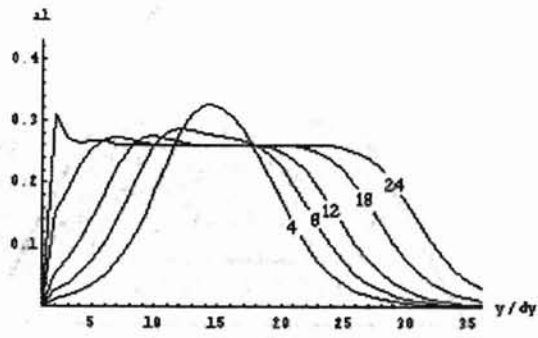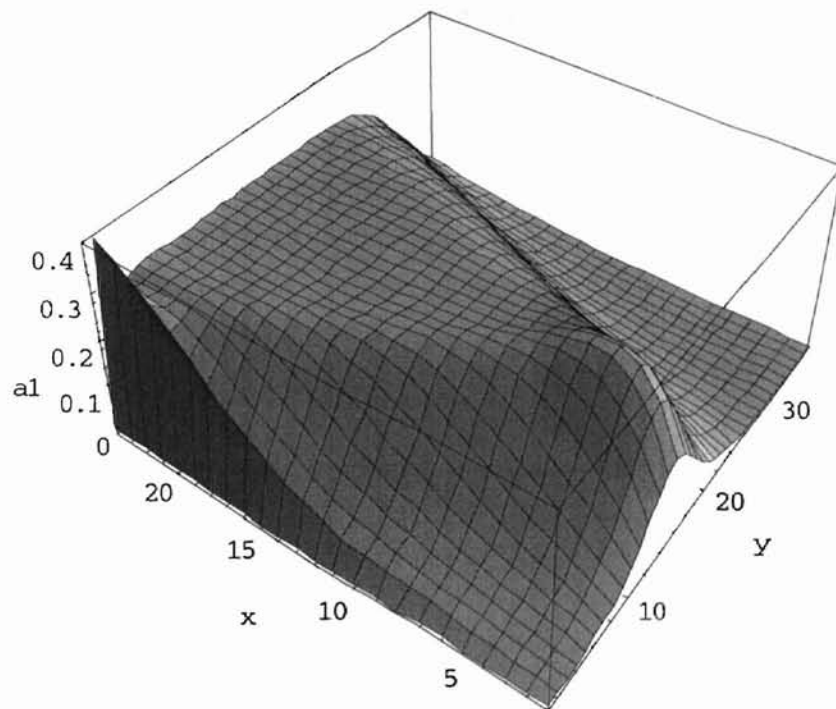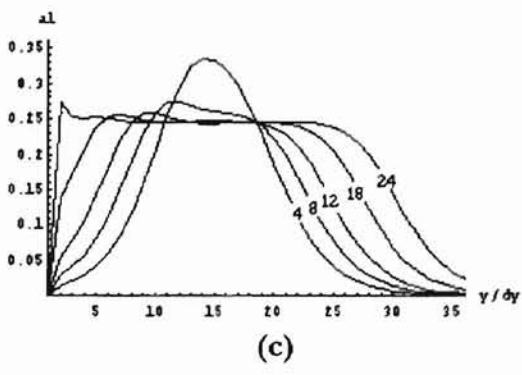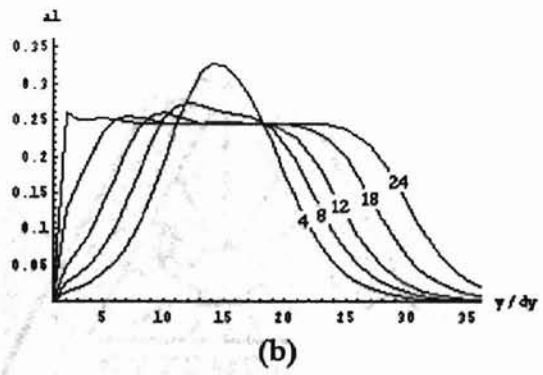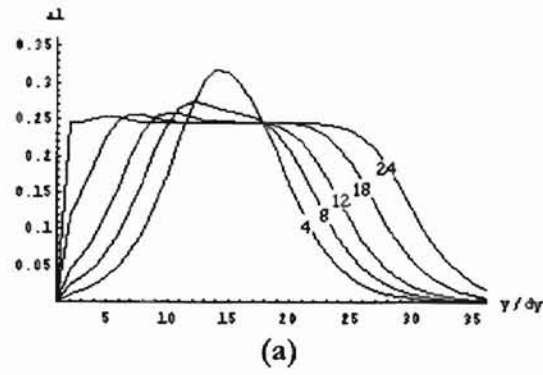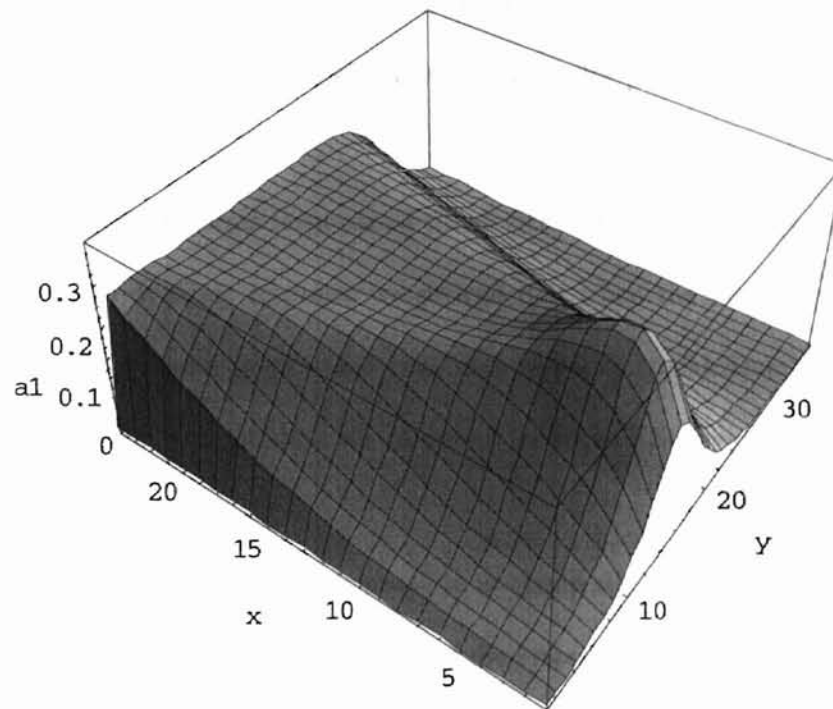**FIGURE 5.9:** The pulse propagation in the device for the case of a secant hyperbolic pulse input where K^2 is 8.605 and $g_0 = 2.3, l_0 = 4.1, A = 0.22, \tau = 4$.

5.4 Conclusions and Suggestions for Future Research

In this thesis we have studied a device consisting of two evanescently coupled waveguides as an all-optical pulse regenerator. One of these waveguides is lossy and the other is amplifying. Both waveguides may exhibit saturation. In this research we show how our proposed device clamps the mode amplitude input to a certain desired value. This value is the critical point of the system which determines the physical parameters and dimensions of our device. This device is inexpensive compared to the presently used techniques for regenerating the optical pulses.

We have studied the dynamic response of the device when arbitrary input excitations are used. By studying the dynamic response we proved that when the saturation intensities of the waveguides are the same (a practical case that helps us to fabricate our device with similar materials for the waveguides) we observed improved behavior (for example, less overshoot).

In this study we also found that it is possible to clamp the mode amplitude to a certain value which is not necessarily the critical point of the system. This clamping is achieved with smaller lengths than what is really needed to reach the critical point. This result is useful also for some cases where it is hard to reach the critical point of the system with reasonable lengths.

While studying the critical point analysis and the stability criteria for the case of dual saturation (where the effects of both loss and gain saturation are considered) we showed that the electrical fields (corresponding to the mode amplitudes in both waveguides) do not incur any extra phase shifts while propagating through the device.

For future work, an experimental effort would certainly be useful. Fabricating this device for cases of interest would help comparing our theoretical results with experimental ones.

This detailed theoretical study and any future experimental study could be useful to explore the possibility of using such inexpensive device in fiber optic telecommunications systems.

In this study we have assumed a constant separation between the waveguides which gives a constant value for the coupling constant along the propagation axis.

In case of a slowly varying separation between the waveguides and assuming that the material properties and all other dimensions are independent of x (i.e., along the propagation axis) the coupling coefficient will be a function of x and may be written as [25]:

$$K(x) = \text{constant} \cdot \exp[-\gamma \cdot d(x)], \tag{5.3}$$

where $d(x)$ represents the separation at any point x and γ is the decay constant of the evanescent fields.

The function $d(x)$ can be written as $d(x) = d_0 + f(x)$, where d_0 is the initial separation at $x = 0$ and $f(x)$ represents the rate of departure of the waveguides from being parallel. Using this representation of $d(x)$, equation (5.3) can be written as

$$K(x) = \text{constant} \cdot \exp[-\gamma \cdot d_0] \cdot \exp[-\gamma \cdot f(x)]. \tag{5.4}$$

Assuming that $K = K_0$ at $x = 0$ we get

$$K_0 = \text{constant} \cdot \exp[-\gamma \cdot d_0],$$

and (5.4) becomes

$$K(x) = K_0 \cdot \exp[-\gamma \cdot f(x)]. \tag{5.5}$$

A more detailed study of our device under the above case will be interesting and could provide a solution for the required $K(x)$ to produce a given output waveform from a given input waveform.

REFERENCES

1. Tingye Li, "The impact of Optical Amplifiers on Long-Distance Lightwave Telecommunicatons," *Proc. IEEE*, vol. 81, No. 11, pp. 1568-1579, November 1993.

2. Jonathan W. Phillips, "Advances Toward an All-Optical Metropolitan Network," 1999 Western Communications Forum, Dallas, TX, February 1999.

3. Thomas H. Wood, "What Architectures Make Sense for Fiber Access Networks?" 1999 Western Communications Forum, Dallas, TX, February 1999.

4. Dave Allen and Wade Saulsberry, "DWDM in the Emerging All-Optical Layer," 1999 Western Communications Forum, Dallas, TX, February 1999.

5. Josepf T. Verdeyen, *Laser Electronics*, 3rd ed., Englewood Cliffs, NJ: Prentice Hall, Inc., 1995.

6. Scott R. Shepard, *An Integrated Optics Pulse Shaping Device*, Massachusetts Institute of Technology, 1981.

7. J. R. Pierce, "Coupling of Mode Propagation," *J. Appl. Phys.*, vol. 25, pp.179-183, 1954.

8. Amnon Yariv, "Coupled-Mode Theory for Guided-Wave Optics," *IEEE J. Quantum Electron.*, vol. QE-9, No. 9, pp. 919-933, September 1973.

9. Y. Yamamoto, T. Kamiya, and H. Yanai, "Improved Coupled Mode Analysis of Corrugated Waveguides and Laser-II: TM Mode," *IEEE J. Quantum Electron.*, vol. QE-14, pp. 620-624, 1978.

10. E. Marcatili, "Improved Coupled-Mode Equations for Dielectric Guides," *IEEE J. Quantum Electron.*, vol. QE-22, pp. 988-993, 1986.

11. L. Tsang and S. L. Chuang, "Improved Coupled-Mode Theory for Reciprocal Anistropic Waveguides," *IEEE J. Lightwave Technol.*, vol. 6, pp. 304-311, 1988.

12. Y. Tomabechi and K. Matsumura, " Improved Analysis for the Coupling Characteristics of Two Rectangular Dielectric Waveguides Laid in Different Layers," *IEEE J. Quantum Electron.*, vol. 24, pp. 2357-2361, 1988.

13. D. Marcuse, "The Coupling of Degenerate Modes in Two Parallel Dielectric Waveguides," *Bell Sys. Tech. J.*, vol. 50, pp. 1791-1816, 1971.

14. A. W. Synder, "Coupling of Modes on a Tapered Dielectric Cylinder," *IEEE Trans. Microwave Theory Tech.*, vol. MTT-18, pp. 383-392, 1970.

15. A. W. Synder, "Coupled Mode Theory for Optical Fibers," *J Opt. Soc. Amer.*, vol. 62, pp. 1267-1277, 1972.

16. A. Yariv and H. F. Taylor, "Guided-Wave Optics," *Proc. IEEE*, vol. 62, pp. 131-134, 1981.

17. G. P. Agrawal, *Nonlinear Fiber Optics*, Boston, MA: Academic, 1989.

18. H. A. Haus and W. Huang, "Coupled-Mode Theory," *Proc. IEEE*, vol. 79, No. 10, pp. 1505-1518, October 1991.

19. H. A. Haus, "Electron Beam Waves in Microwave Tubes," *Proc. Symp. Electronic Waveguides*, Polytechnic Institute of Brooklyn, Apr. 8-10, 1958.

20. Yariv, *Optical Electronics in Modern Communications*, 5th ed., New York: Oxford University Press, Inc., 1997.

21. R. H. Pantell and H. E. Puthoff, *"Fundamentals of Quantum Electronics,"* New York: Wiley, 1969.

22. D. W. Jordan and P. Smith, *Nonlinear Ordinary Differential Equations*, 2nd ed. New York: Oxford University Press, Inc., 1987.

23. Stephan Wolfram, *Mathematica*, 2nd ed. Redwood City: Addison-Wesley Publishing Co., 1991.

24. William F. Ames, *Numerical Methods for Partial Differential Equations*, San Diego: Academic Press, Inc., 1992.

25. Talal Findakly and Chin-Lin Chen, "Optical Directional Couplers with Variable Spacing," *App. Opt.*, vol. 17, No. 5, pp. 769-773, March 1978.

APPENDIX A

```
ClearAll[x,y,jac,r,q,eig1,g,k,l,eig2,mat,sol,x1,x2,eigenvalues,cpx,cpy,u,v]

l=5.;g=2.;

r[x_,y_]=-l*y/(1+y^2)-k*x;

q[x_,y_]=g*x/(1+x^2)+k*y;

For[i=1,i<1000,k=Sqrt[i/100];sol=Solve[{r[x,y]==0,q[x,y]==0},{x,y}];

  jac={{D[q[x,y],x],D[q[x,y],y]},{D[r[x,y],x],D[r[x,y],y]}};

  mat=MatrixForm[jac];cpx=x/.N[sol];cpy=y/.N[sol];x1=Extract[cpx,1];

  y1=Extract[cpy,1];cx[i]=x1;x=x1;y=y1;eigenvalues=Eigenvalues[jac];

  exr1=Extract[eigenvalues,1];exr2=Extract[eigenvalues,2];re1=Re[exr1];

  im1=Im[exr1];ret1[i]=re1;imt1[i]=im1;re2=Re[exr2];im2=Im[exr2];ret2[i]=re2;

  imt2[i]=im2;

  ClearAll[x,y,x1,y1,sol,jac,mat,eigenvalues,cpx,cpy,k,re1,im1,re2,im2];i+=1]

u1=Table[ret1[j],{j,1,999}];

v1=Table[imt1[j],{j,1,999}];

u2=Table[ret2[j],{j,1,999}];

v2=Table[imt2[j],{j,1,999}];

lst1=ListPlot[u1,PlotJoined->True,AxesLabel->{"100k","Re1"}];

lst2=ListPlot[v1,PlotJoined->True,AxesLabel->{"100k","Im1"}];

lst3=ListPlot[u2,PlotJoined->True,AxesLabel->{"100k","Re2"}];

lst4=ListPlot[v2,PlotJoined->True,AxesLabel->{"100k","Im2"}];

Show[GraphicsArray[{{lst1,lst3},{lst2,lst4}}]]
```

APPENDIX B

```
ClearAll[x,y,jac,r,q,eig1,g,k,l,eig2,mat,sol,x1,x2,eigenvalues,cpx,cpy]

l=5.5;

g=3.5;

k=Sqrt[18.7332];

r[x_,y_]=-l*y/(1+y^2)-k*x;

q[x_,y_]=g*x/(1+x^2)+k*y;

sol=Solve[{r[x,y]==0,q[x,y]==0},{x,y}];

jac={{D[q[x,y],x],D[q[x,y],y]},{D[r[x,y],x],D[r[x,y],y]}};

mat=MatrixForm[jac];

cpx=x/.N[sol];

cpy=y/.N[sol];

x1=Extract[cpx,1];

y1=Extract[cpy,1];

Print["Critical points are->",sol]

x=x1;

y=y1;

eigenvalues=Eigenvalues[jac];

Print["Eigenvalues are->",eigenvalues]
```

APPENDIX C

```
<<Graphics`PlotField`

ClearAll[t,a,b,pvc,eqone,eqtwo,x,y];

Array[a,{11,11}];

eqone=2.3x/(1+x^2)+Sqrt[9.695]y;

eqtwo=-5y/(1+y^2)-Sqrt[9.695]x;

pvc=PlotVectorField[{eqone,eqtwo},{x,-1,1},{y,-1,1},Axes->Automatic,

    AxesOrigin->{0,0},AxesLabel->{a1,a2},DisplayFunction->Identity]

For[i=1,i<12,For[j=1,j<12,

        a[i,j] = NDSolve[{x'[t]==2.3x[t]/(1+x[t]^2) +Sqrt[9.695]y[t],

        y'[t] ==-5y[t]/(1+y[t]^2)-Sqrt[9.695]x[t],

        x[0]== (0.2i-1.2), y[0]==(0.2j-1.2)}, {x,y},{t,0,0.6}]

        ;j++];i++]

Array[b,{11,11}];

For[i=1,i<12,For[j=1,j<12,

        b[i,j] =

    ParametricPlot[

        Evaluate[{x[t], y[t]} /.a[i,j]],{t,0,0.6},

        PlotRange->{{-1,1},{-1,1}},DisplayFunction->Identity,

        AxesLabel->{a1,a2}];j++];i++]

lst1=ListPlot[Table[{-0.354n,0.232},{n,1}],Prolog->AbsolutePointSize[5],

    DisplayFunction->Identity];

lst2=ListPlot[Table[{0.354n,-0.232},{n,1}],Prolog->AbsolutePointSize[5],
```

```
          DisplayFunction->Identity];

lst3=ListPlot[Table[{0n,0},{n,1}],Prolog->AbsolutePointSize[5],

   DisplayFunction->Identity];

 Array[t,{11,11}];

 For[i=1,i<12,For[j=1,j<12,If[i==1,

 If [j==1,t[i,j]=Show[{b[i,1],b[i,2]},PlotRange->All

 ,DisplayFunction->Identity],

 If[j==11,t[i,11]=Show[{t[i,10],b[i,j]},PlotRange->All

 ,DisplayFunction->Identity],

 t[i,j]=Show[{t[i,j-1],b[i,j+1]},PlotRange->All,

 DisplayFunction->Identity]]],

 If [j==1,t[i,j]=Show[{t[i-1,11],b[i,j]},PlotRange->All,

 DisplayFunction->Identity],

 If[j==11,t[i,11]=Show[{t[i,10],b[i,j]},PlotRange->All,

 DisplayFunction->Identity],

 t[i,j]= Show[{t[i,j-1],b[i,j]}, PlotRange->All,

 DisplayFunction->Identity]]]] ;j++];i++]

    Show[{t[11,11],lst1,lst2,lst3},PlotRange->{{-1,1},{-1,1}},

       DisplayFunction->$DisplayFunction,AspectRatio->1,

       Prolog->AbsolutePointSize[5]];

   Show[{pvc,lst1,lst2,lst3},PlotRange->{{-1,1},{-1,1}},AspectRatio->1,

      DisplayFunction->$DisplayFunction,Prolog->AbsolutePointSize[5]];
```

APPENDIX D

```
Clear[r,s,t,u,sol];

sol=NDSolve[{r'[z]==2r[z]/(1+r[z]^2+s[z]^2)+Sqrt[8.505]t[z],

    s'[z]==2s[z]/(1+r[z]^2+s[z]^2)+Sqrt[8.505]u[z],

        t'[z]==-5t[z]/(1+t[z]^2+u[z]^2)-Sqrt[8.505]r[z],

            u'[z]==-5u[z]/(1+t[z]^2+u[z]^2)-Sqrt[8.505]s[z],r[0]==1,s[0]==0,t[0]==2,

    u[0]==0},{r,s,t,u},{z,0,10}];

par=ParametricPlot3D[Evaluate[{z,r[z],s[z]}/.sol],{z,0,10},

    ViewPoint->{-2.320, 2.288, 0.910},AxesLabel->{z,r,s},PlotPoints->200,

    BoxRatios->{2,1,1},PlotRange->All]

par=ParametricPlot3D[Evaluate[{z,t[z],u[z]}/.sol],{z,0,10},

    ViewPoint->{-2.320, 2.288, 0.910},AxesLabel->{z,t,u},PlotPoints->200,

    BoxRatios->{2,1,1},PlotRange->All]

ParametricPlot[Evaluate[{r[z],t[z]}/.sol],{z,0,10},PlotRange->All]
```

APPENDIX E

```
<<Graphics`PlotField`

ClearAll[t,a,b,pvc,eqone,eqtwo,x,y,c,d,r,s,lst1,d,c];

Array[a,{7,1}];

For[i=1,i<8,For[j=1,j<2,

        a[i,j] = NDSolve[{x'[t]==5x[t]/(1+x[t]^2) +Sqrt[6.9]y[t],

    y'[t] ==-6y[t]/(1+y[t]^2)-Sqrt[6.9]x[t],

    x[0]== (-0.1i-1), y[0]==0}, {x,y},{t,0,.654}];j++];i++]

For[i=1,i<8,w[i]=x[0.654]/.a[i,1];z[i]=y[0.654]/.a[i,1];i++]

Array[b,{7,1}];

For[i=1,i<8,For[j=1,j<2,

        b[i,j] =ParametricPlot[Evaluate[{x[t], y[t]} /.a[i,j]],{t,0,.654},

    PlotRange->{{-2.5,0},{0,2.5}},DisplayFunction->Identity,

    AxesLabel->{a1,a2}];j++];i++]

lst1=ListPlot[Table[{-1.14n,0.94},{n,1}],Prolog->AbsolutePointSize[5]];

Show[{b[1,1],b[2,1],b[3,1],b[4,1],b[5,1],b[6,1],b[7,1],lst1},

  PlotRange->{{-2.5,0.5},{-0.5,2.5}},AxesOrigin->{-2.5,0},

  DisplayFunction->$DisplayFunction,AspectRatio->1]
```

APPENDIX F

ClearAll[dif,dift,difj,plot,m,n,j,k,u,v,pxy,plt,x,y,sx,sy]

For[j=9,j<16,sol=NDSolve[{x'[t] == 5x[t]/(1+(x[t]^2)) +Sqrt [5.55]y[t],

    y'[t] ==-2y[t]/(1+y[t]^2)-Sqrt[5.55]x[t],

    x[0]== -j/10, y[0]==0}, {x,y},{t,0,.641}];m=x[0]/.sol;

  k=Extract[m,1];n=x[.641]/.N[sol];finalx=Extract[n,1];l=y[.641]/.N[sol];

  finaly=Extract[l,1];sx[j]=finalx;sy[j]=finaly;pxy[j]=Table[{sx[j],sy[j]}];

  dif=k-finalx;plot[j]=dif;j++]

v=Table[pxy[j],{j,9,15}];

ListPlot[v,PlotJoined->True,PlotRange->{{0,-2.5},{0,2.5}},AspectRatio->1,

  AxesLabel->{a1,a2},AxesOrigin->{-2.5,0}];

APPENDIX G

```
Clear[m,n,dy,ds,p,g,a10t,a20t,tao,l0t,a1t,a2t,lt,a1ft,a2ft,lft,a,b,c,d,u,v,w,
   x,t,r,y,k,s,sol,l,a1,a2,l0,a10,a20,zf,zt,z,o]

n=16;

f=1;

tao=4;

m=36;

ds=0.4;

dy=6*tao/(15);

p=4.1;

g=2.3;

k=Sqrt[8.305];

a10t=Table[a10,{i,1},{j,m}];

a20t=Table[a20,{i,1},{j,m}];

l0t=Table[l0,{i,1},{j,m}];

z0t=Table[z0,{i,1},{j,m}];

a1t=Table[a1,{i,n-1},{j,m-1}];

a2t=Table[a2,{i,n-1},{j,m-1}];

lt=Table[l,{i,n-1},{j,m-1}];

zt=Table[z,{i,n-1},{j,m-1}];

a1ft=Table[a1f,{i,n},{j,m}];

a2ft=Table[a2f,{i,n},{j,m}];

lft=Table[lf,{i,n},{j,m}];
```

```
zft=Table[zf,{i,n},{j,m}];

ct=Table[c,{i,m}];

dt=Table[d,{i,m}];

et=Table[e,{i,m}];

ht=Table[h,{i,m}];

For[j=1,j<m+1,a10t[[1,j]]=0.18*Sech[0.8844(j*dy-6*tao)/tao];j++]

For[j=1,j<m+1,a20t[[1,j]]=0;j++]

For[j=1,j<m+1,l0t[[1,j]]=1;j++]

For[j=1,j<m+1,z0t[[1,j]]=1;j++]

For[i=1,i<n,

  For[j=1,j<m,

    If[i==1,If[j==1,y=a10t[[1,j+1]];s=a20t[[1,j+1]];u=1;v=1;w=1;q=1;b=1;o=1;

      sol=Solve[{x-y-ds*g*x*z-ds*k*r==0,

          11 t-18 u+9 v-2 w+6 dy*t*(1+r^2)-6 dy==0,

          11 z-18 q+9 b-2 o+6 dy*z*(1+(x^2)/f)-6 dy==0,

          r-s+ds*p*t*r+ds*k*x==0},{x,r,t,z}];ct=x/.N[sol];dt=r/.N[sol];

      et=t/.N[sol];ht=z/.N[sol];a1t[[i,j]]=Extract[ct,7];

      a2t[[i,j]]=Extract[dt,7];lt[[i,j]]=Extract[et,7];

      zt[[i,j]]=Extract[ht,7],

      If[j==2,y=a10t[[1,j+1]];s=a20t[[1,j+1]];u=lt[[i,j-1]];v=1;w=1;

        q=zt[[i,j-1]];b=1;o=1;

        sol=Solve[{x-y-ds*g*x*z-ds*k*r==0,

            11 t-18 u+9 v-2 w+6 dy*t*(1+r^2)-6 dy==0,

            11 z-18 q+9 b-2 o+6 dy*z*(1+(x^2)/f)-6 dy==0,
```

79

r-s+ds*p*t*r+ds*k*x==0},{x,r,t,z}];ct=x/.N[sol];dt=r/.N[sol];

et=t/.N[sol];ht=z/.N[sol];a1t[[i,j]]=Extract[ct,7];

a2t[[i,j]]=Extract[dt,7];lt[[i,j]]=Extract[et,7];

zt[[i,j]]=Extract[ht,7],

If[j==3,y=a10t[[1,j+1]];s=a20t[[1,j+1]];u=lt[[i,j-1]];v=lt[[i,j-2]];

 w=1;q=zt[[i,j-1]];b=zt[[i,j-2]];o=1;

 sol=Solve[{x-y-ds*g*x*z-ds*k*r==0,

     11 t-18 u+9 v-2 w+6 dy*t*(1+r^2)-6 dy==0,

     11 z-18 q+9 b-2 o+6 dy*z*(1+(x^2)/f)-6 dy==0,

     r-s+ds*p*t*r+ds*k*x==0},{x,r,t,z}];ct=x/.N[sol];

 dt=r/.N[sol];et=t/.N[sol];ht=z/.N[sol];a1t[[i,j]]=Extract[ct,7];

 a2t[[i,j]]=Extract[dt,7];lt[[i,j]]=Extract[et,7];

 zt[[i,j]]=Extract[ht,7],y=a10t[[1,j+1]];s=a20t[[1,j+1]];

 u=lt[[i,j-1]];v=lt[[i,j-2]];w=lt[[i,j-3]];q=zt[[i,j-1]];

 b=zt[[i,j-2]];o=zt[[i,j-3]];

 sol=Solve[{x-y-ds*g*x*z-ds*k*r==0,

     11 t-18 u+9 v-2 w+6 dy*t*(1+r^2)-6 dy==0,

     11 z-18 q+9 b-2 o+6 dy*z*(1+(x^2)/f)-6 dy==0,

     r-s+ds*p*t*r+ds*k*x==0},{x,r,t,z}];ct=x/.N[sol];

 dt=r/.N[sol];et=t/.N[sol];ht=z/.N[sol];a1t[[i,j]]=Extract[ct,7];

 a2t[[i,j]]=Extract[dt,7];lt[[i,j]]=Extract[et,7];

 zt[[i,j]]=Extract[ht,7]]]],y=a1t[[i-1,j]];s=a2t[[i-1,j]];

If[j==1,u=1;v=1;w=1;q=1;b=1;o=1;

 sol=Solve[{x-y-ds*g*x*z-ds*k*r==0,

11 t-18 u+9 v-2 w+6 dy*t*(1+r^2)-6 dy==0,

　　11 z-18 q+9 b-2 o+6 dy*z*(1+(x^2)/f)-6 dy==0,

　　r-s+ds*p*t*r+ds*k*x==0},{x,r,t,z}];ct=x/.N[sol];dt=r/.N[sol];

et=t/.N[sol];ht=z/.N[sol];a1t[[i,j]]=Extract[ct,7];

a2t[[i,j]]=Extract[dt,7];lt[[i,j]]=Extract[et,7];

zt[[i,j]]=Extract[ht,7],

If[j==2,u=lt[[i,j-1]];v=1;w=1;q=zt[[i,j-1]];b=1;o=1;

　sol=Solve[{x-y-ds*g*x*z-ds*k*r==0,

　　　11 t-18 u+9 v-2 w+6 dy*t*(1+r^2)-6 dy==0,

　　　11 z-18 q+9 b-2 o+6 dy*z*(1+(x^2)/f)-6 dy==0,

　　　r-s+ds*p*t*r+ds*k*x==0},{x,r,t,z}];ct=x/.N[sol];dt=r/.N[sol];

　et=t/.N[sol];ht=z/.N[sol];a1t[[i,j]]=Extract[ct,7];

　a2t[[i,j]]=Extract[dt,7];lt[[i,j]]=Extract[et,7];

　zt[[i,j]]=Extract[ht,7],

　If[j==3,u=lt[[i,j-1]];v=lt[[i,j-2]];w=1;q=zt[[i,j-1]];b=zt[[i,j-2]];

　　o=1;sol=Solve[{x-y-ds*g*x*z-ds*k*r==0,

　　　　11 t-18 u+9 v-2 w+6 dy*t*(1+r^2)-6 dy==0,

　　　　11 z-18 q+9 b-2 o+6 dy*z*(1+(x^2)/f)-6 dy==0,

　　　　r-s+ds*p*t*r+ds*k*x==0},{x,r,t,z}];ct=x/.N[sol];

　dt=r/.N[sol];et=t/.N[sol];ht=z/.N[sol];a1t[[i,j]]=Extract[ct,7];

　a2t[[i,j]]=Extract[dt,7];lt[[i,j]]=Extract[et,7];

　zt[[i,j]]=Extract[ht,7],u=lt[[i,j-1]];v=lt[[i,j-2]];w=lt[[i,j-3]];

　q=zt[[i,j-1]];b=zt[[i,j-2]];o=zt[[i,j-3]];

　sol=Solve[{x-y-ds*g*x*z-ds*k*r==0,

$$11\ t\text{-}18\ u+9\ v\text{-}2\ w+6\ dy*t*(1+r\char94 2)\text{-}6\ dy==0,$$

$$11\ z\text{-}18\ q+9\ b\text{-}2\ o+6\ dy*z*(1+(x\char94 2)/f)\text{-}6\ dy==0,$$

$$r\text{-}s+ds*p*t*r+ds*k*x==0\},\{x,r,t,z\}];ct=x/.N[sol];$$

dt=r/.N[sol];et=t/.N[sol];ht=z/.N[sol];a1t[[i,j]]=Extract[ct,7];

a2t[[i,j]]=Extract[dt,7];lt[[i,j]]=Extract[et,7];

zt[[i,j]]=Extract[ht,7]]]]];j++];i++]

a11t2=Extract[a1t,1];

a1ft2=Insert[a11t2,0,2];

a11t4=Extract[a1t,4];

a1ft4=Insert[a11t4,0,1];

a11t6=Extract[a1t,6];

a1ft6=Insert[a11t6,0,1];

a11t8=Extract[a1t,8];

a1ft8=Insert[a11t8,0,1];

a11t10=Extract[a1t,10];

a1ft10=Insert[a11t10,0,1];

a11t12=Extract[a1t,12];

a1ft12=Insert[a11t12,0,1];

a11t14=Extract[a1t,14];

a1ft14=Insert[a11t14,0,1];

a11t16=Extract[a1t,16];

a1ft16=Insert[a11t16,0,1];

lst2=ListPlot[a1ft2,PlotJoined->True,PlotRange->All,

DisplayFunction->Identity];

```
lst4=ListPlot[a1ft4,PlotJoined->True,PlotRange->All,

   DisplayFunction->Identity];

lst6=ListPlot[a1ft6,PlotJoined->True,PlotRange->All,

   DisplayFunction->Identity];

lst8=ListPlot[a1ft8,PlotJoined->True,PlotRange->All,

   DisplayFunction->Identity];

lst10=ListPlot[a1ft10,PlotJoined->True,PlotRange->All,

   DisplayFunction->Identity];

lst12=ListPlot[a1ft12,PlotJoined->True,PlotRange->All,

   DisplayFunction->Identity];

lst14=ListPlot[a1ft14,PlotJoined->True,PlotRange->All,

   DisplayFunction->Identity];

lst16=ListPlot[a1ft16,PlotJoined->True,PlotRange->All,

   DisplayFunction->Identity];

Show[{lst2,lst4,lst6,lst8},DisplayFunction->$DisplayFunction,PlotRange->All,

 AxesOrigin->{1,0}]

Show[{lst10,lst12,lst14,lst16},DisplayFunction->$DisplayFunction,

 PlotRange->All,AxesOrigin->{1,0}]
```

APPENDIX H

```
Clear[f,dif,eq1,eq2,x,y,m,n,x1,x2,sol1,sol2]

eq1=2x/(1+(x^2)/f)+Sqrt[8.505]y;

eq2=-5.y/(1+y^2)-Sqrt[8.505]x;

For[f=1,f<21,sol1=Solve[{eq1==0,eq2==0},{x,y}];

  sol2=Solve[{2x+Sqrt[8.505]y==0,eq2==0},{x,y}];x1=x/.sol1;m=Extract[x1,1];

  x2=x/.sol2;n=Extract[x2,1];dif[f]=m-n;f++]

u=Table[dif[f],{f,1,20}];

ListPlot[u,PlotJoined->True,AxesLabel->{"f","diff"},AxesOrigin->{1,0}]
```

VITA ²

Najeeb Farhan Haddad

Candidate for the Degree of

Master of Science

Thesis: AN ALL-OPTICAL PULSE REGENERATOR

Major Field: Electrical Engineering.

Personal Data: Born in Al-Wahadneh, Jordan, on December 19, 1969, the son of Farhan and Iskanderiah Haddad.

Education: Graduated from Ajloun High School, Ajloun, Jordan in June 1987; received Bachelor of Science degree in Electrical Engineering from Mu'tah University, Mu'tah, Jordan 1991; Completed the requirements for the Master of Science degree with a major in Electrical Engineering at Oklahoma State University in May 1999.

Experience: Worked as a Telecommunication Engineer in the Royal Jordanian Air Force, Jordan, June 1991 to September 1997; worked as a teaching assistant in Jordan University of Science and Technology, Jordan, September 1997 to January 1998; worked as a research assistant in the Electrical and Computer Engineering Department at Oklahoma State University, August 1998 to December 1998.

Professional Membership: IEEE student member; IEEE Laser and Electro-Optic Society student member; Jordanian Council for Engineers.